Annual Review of Materials Research

Ternary Nitride Materials: Fundamentals and Emerging Device Applications

Ann L. Greenaway,[1] Celeste L. Melamed,[1,2] M. Brooks Tellekamp,[1] Rachel Woods-Robinson,[1,3,4] Eric S. Toberer,[2] James R. Neilson,[5] and Adele C. Tamboli[1,2]

[1]Materials, Chemical, and Computational Science Directorate, National Renewable Energy Laboratory, Golden, Colorado 80401, USA; email: adele.tamboli@nrel.gov

[2]Department of Physics, Colorado School of Mines, Golden, Colorado 80401, USA

[3]Applied Science and Technology Graduate Group, University of California, Berkeley, California 97402, USA

[4]Energy Technologies Area, Lawrence Berkeley National Laboratory, Berkeley, California 94720, USA

[5]Department of Chemistry, Colorado State University, Fort Collins, Colorado 80523, USA

Annu. Rev. Mater. Res. 2021. 51:13.1–13.28

The *Annual Review of Materials Research* is online at matsci.annualreviews.org

https://doi.org/10.1146/annurev-matsci-080819-012444

Keywords

ternary nitride, structural chemistry, metastability, nitride synthesis, optoelectronics, battery

Abstract

Interest in inorganic ternary nitride materials has grown rapidly over the past few decades, as their diverse chemistries and structures make them appealing for a variety of applications. Due to synthetic challenges posed by the stability of N_2, the number of predicted nitride compounds dwarfs the number that have been synthesized, offering a breadth of opportunity for exploration. This review summarizes the fundamental properties and structural chemistry of ternary nitrides, leveraging metastability and the impact of nitrogen chemical potential. A discussion of prevalent defects, both detrimental and beneficial, is followed by a survey of synthesis techniques and their interplay with metastability. Throughout the review, we highlight applications (such as solid-state lighting, electrochemical energy storage, and electronic devices) in which ternary nitrides show particular promise.

1. INTRODUCTION

Ternary inorganic nitride: a compound consisting of two metal cations and the nitrogen anion; this review focuses on emerging compounds in this class rather than on heavily investigated alloys such as $In_xGa_{1-x}N$

Chemical hardness: quantification of the soft/hard acid/base concept, where soft acids are acceptor atoms with large, diffuse, polarizable electron clouds and easily excited outer electrons, and hard acids have the inverse properties

Nitride materials surged in importance during the twentieth century as numerous applications were identified from technologies ranging from light-emitting diodes (LEDs), lasers, and power electronics to superconductors and hard coatings. As the utility of nitrides increased, so did the need for broader structure–property tunability, spurring the development of ternary nitride research. The nitrogen atom in the solid state presents both a promise and a challenge: Its strong bonds lead to compelling materials properties and long experimental lifetimes but make synthesis challenging because of the relative inertness of N_2. Despite the prevalence of nitrogen on Earth (1), there are few reported ternary nitrides compared with ternary oxides, making this a promising field for research (2, 3).

Ternary nitrides were sparsely studied from the 1950s through the 1980s (**Figure 1*a*,*c***); early work by a handful of research groups was limited to synthesis and fundamental structural characterization (4–7). In the 1990s, interest in ternary nitrides increased as techniques such as solid-state metathesis, ball milling in a nitrogen atmosphere, microwave-generated nitrogen plasmas, and novel molecular and oxide precursors were used in exploratory syntheses (8–14). This expansion has continued into the twenty-first century, with progress in the development of previously synthesized nitrides for applications varying from hydrogen storage to photovoltaic absorbers and LEDs (15–17), as well in as the continued search for new ternary nitrides, driven by the rise of computational materials prediction and discovery (2, 3, 18). Interest in ternary nitrides has led to a commensurate increase in their elemental diversity (**Figure 1*b***), expanding this space to an exciting array of potential chemistries.

In this review, we describe how the diversity of the nitride chemistry enables a wide breadth of structures and properties, reaching beyond established application spaces where binary nitrides have historically been used. New applications are emerging in which ternary nitrides can uniquely serve, such as batteries and phosphors. Many of these potential applications are still theoretical or in an early stage: There is a huge opportunity space for device-oriented materials research in ternary nitrides. We highlight the unusual metastability of ternary nitrides and their ability to be integrated into hybrid devices with binary nitrides. We discuss how the particular defect chemistry of ternary nitrides plays into properties such as cation site disorder and anion vacancies, leading to some challenges and some opportunities for applications.

2. FUNDAMENTAL PROPERTIES AND STRUCTURAL CHEMISTRY

Inorganic ternary nitrides span a broad range of compositions (**Figure 1*b***) and stoichiometries, yielding a commensurate breadth of properties. This chemical diversity can be traced to the unusual properties of nitrogen. In the following subsections, we discuss the solid-state chemistry of nitrides, addressing the behavior of nitrogen as well as cation chemistries and metastability, and highlighting recent examples of compounds that continue to expand our understanding of these materials.

2.1. Nitrogen in the Solid State

To understand the nitrogen anion, it is illustrative to compare it with other nonmetal elements. **Figure 2*a*** depicts electronegativity and absolute hardness across the p-block elements. Nitrogen is very electronegative (comparable to chlorine, but less so than oxygen and fluorine) (19), with its electronegativity arising from its poorly shielded nucleus. For this reason, nitrogen is the hardest element of the anion-forming main group elements (20). Its high chemical hardness and intermediate electronegativity give rise to nitrogen's unique properties, such that it can form

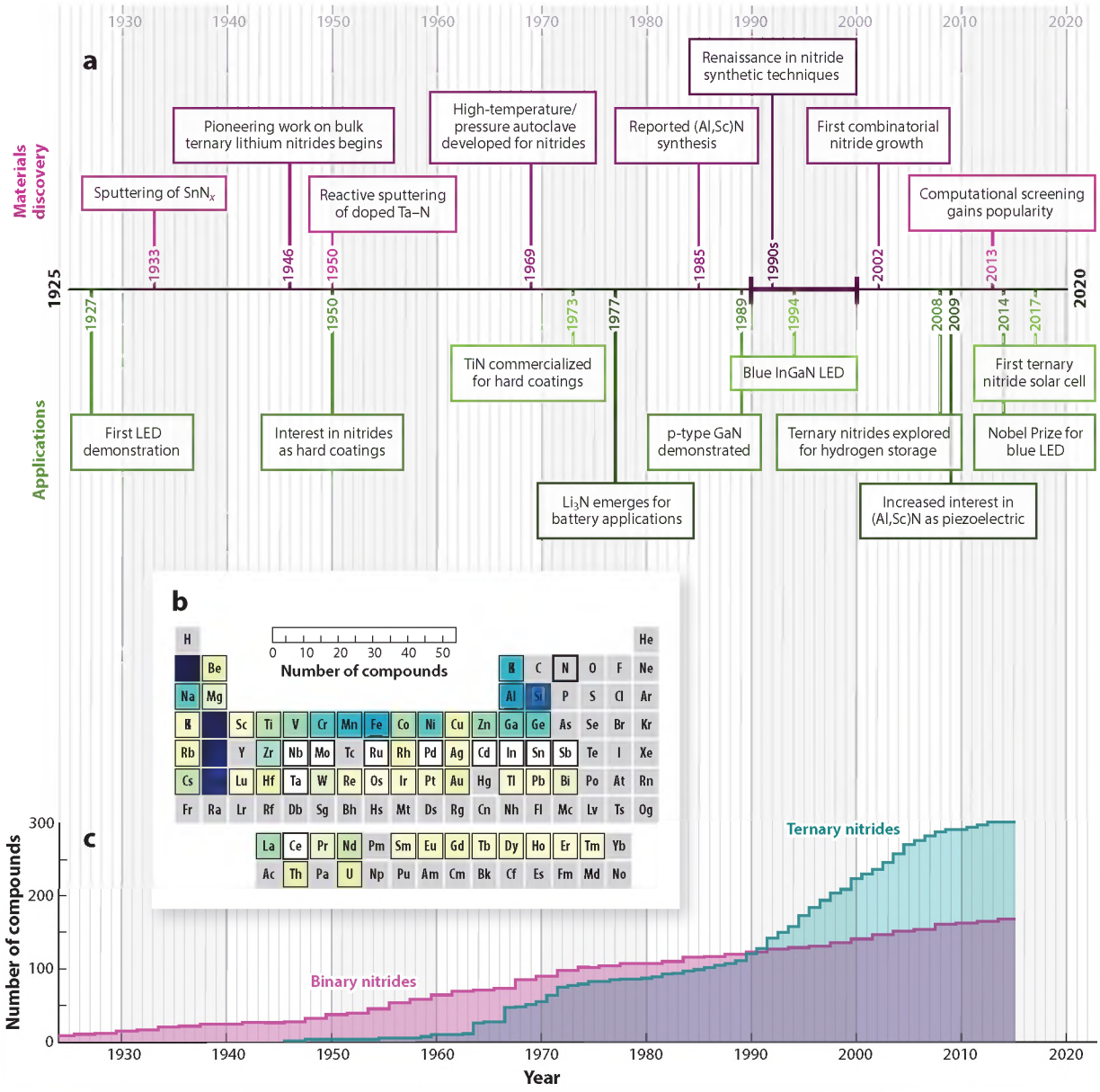

Figure 1

(*a*) A timeline of important events in nitride research, divided between materials discovery and developments in applications. (*b*) A heat map of the frequency of elements in fully ordered ternary nitrides, as reported in the Inorganic Crystal Structure Database (ICSD). Compounds where nitrogen was not the sole anion were removed from the list. (*c*) A histogram of all experimentally synthesized binary and ternary nitride compounds (with nitrogen as the sole anion) over time, from the ICSD. Each compound refers to a unique crystal structure, and the compound's year refers to the earliest report of each compound. Additional information for all sections can be found in section S2 of the **Supplemental Material**. Abbreviation: LED, light-emitting diode.

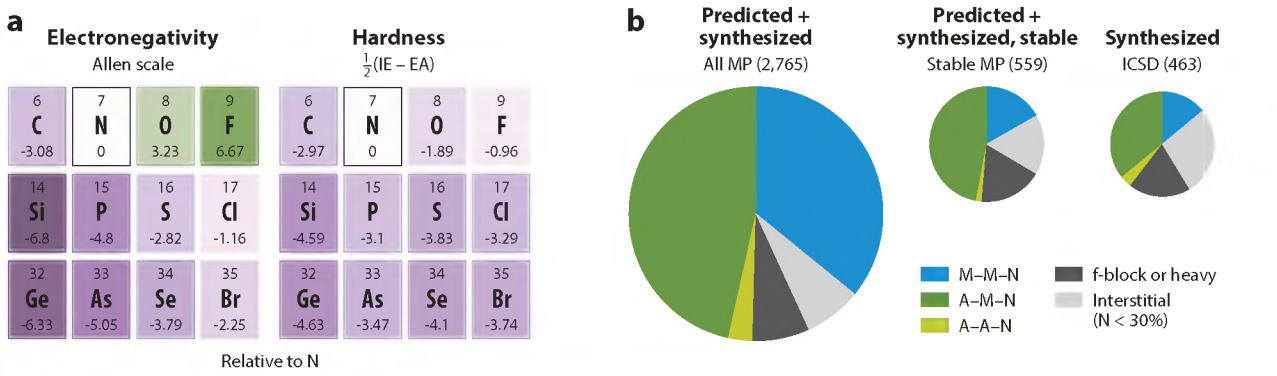

Figure 2

(*a*) Comparison of electronegativity and hardness [determined utilizing ionization energy (IE) and electron affinity (EA)] of common anions relative to the values for nitrogen. (*b*) Comparison of chemical distributions of ternary nitrides across materials databases. Only unique compounds are counted for each pie chart, for all of the Materials Project (MP), the thermodynamically stable compounds in the MP (E_{hull} = 0 eV/atom), and the experimental Inorganic Crystal Structure Database (ICSD). Further details can be found in section S3 of the **Supplemental Material**.

high-coordination ionic compounds as well as covalent bonds as a result of its large, delocalized electron cloud in the formal anion, N^{3-}.

This unique combination of hardness and electronegativity allows nitrogen to adopt various bond hybridizations (and, therefore, bonding geometries) in the solid state (21), enabling coordination numbers from two to eight, although six is the most common (7, 8, 22). Nitrogen also represents a middle ground of bonding between anions: Its variable bond character enables, on the one hand, better orbital overlap with metals than oxygen, resulting in smaller bandgap semiconductors (2), and, on the other hand, compounds with metallic conductivity similar to that of carbides (23). Furthermore, there are examples of nitrogen adopting multiple bond geometries within the same compound (14, 24). This variability in bond hybridization and mixed ionic–covalent character, as well as high polarizability of the nitrogen anion (25), affords highly cohesive materials with a large structural diversity (26, 27).

2.2. Cation Chemistries

Ternary nitrides form, or are predicted to form, with metals from across the periodic table (**Figure 1*b***). While elemental nitrogen has a high chemical hardness, the addition of electron density creates a rather polarizable anion, thus leading to immense structural diversity with different cations. However, because of the challenges of ternary nitride synthesis, discussed in detail in Section 4, the number of experimentally known materials in this category is dwarfed by the number of predicted compounds. Illustrating the compositional variability of ternary nitrides, **Figure 2*b*** plots the prevalence of five nitride classes across two materials databases (additional comparisons can be found in section S3 of the **Supplemental Material**). The first three classes are the focus of this review: *M*–*M*–N, *A*–*M*–N, and *A*–*A*–N, where *A* is an alkali or alkaline earth metal and *M* is a transition or p-block metal, following Sun et al. (3). The statistics presented in the figure include multiple instances of compounds within the same chemistry system [e.g., Zn_3MoN_4 and $ZnMoN_2$ (28) in the system Zn–Mo–N]. The categorization f-block or heavy designates compounds containing any lanthanide (lanthanum to ytterbium) or element with an atomic number greater than 83 (bismuth), while the interstitial class designates materials with ≤20% atomic nitrogen in their formula.

While the distribution of predicted ternary nitrides varies across databases, it is clear that *A*–*M*–N compounds form a plurality of predictions and entries in the experimental Inorganic Crystal Structure Database (ICSD). Many of the earliest-discovered ternary nitrides were based around strongly electropositive metals such as lithium, including LiZnN and Li_3AlN_2 (4), which stabilize compounds through the inductive effect (3, 22). In contrast, *A*–*A*–N compounds are the smallest portion of compounds across databases, because of difficulty stabilizing multiple electropositive metal cations (3). The proportion of *M*–*M*–N compounds varies widely across databases and, for the Materials Project (MP), is substantially reduced when only stable compounds are considered. However, this value is close to the number of *M*–*M*–N compounds in the ICSD, an indication of the historical challenge of synthesizing ternary nitrides with less electropositive metal cations. This distribution both sheds light on historical challenges in nitride discovery and indicates rich opportunities for synthesis of new nitrides, particularly in the *M*–*M*–N space, which, as described in Section 2.4, is generally metastable.

2.3. Structural Chemistries

The combination of nitrogen's chemical properties and the range of cations with which it can form bonds leads to wide structural variety in ternary nitrides. Taken together, these factors enable nitrogen to form in more diverse structural types, particularly for ternary materials, than are observed for other anions, including unique structures with no counterparts in other anion systems [e.g., layered $P6_3/mcm$ Ca_6MN_5, where M = Ga, Mn, or Fe (26)]. **Figure 3** shows a sample of these structures, many of which are of particular interest for technological applications. The wurtzite family (**Figure 3*a***) is derived from group III nitride materials by cation mutation (29, 30); similarly, the rocksalt family (**Figure 3*b***) is analogous to binary rocksalts such as TiN. Cation-ordered structures for these materials appear in computational structure predictions, but cation-disordered structures are often observed experimentally (31), as illustrated in the figure. Both of these classes are interesting for technological applications because of their potential for heteroepitaxial integration with widely used binary nitrides while enabling wider property spaces, as discussed in Section 4.4. Antiperovskites (**Figure 3*c***) are common structures for ternary nitrides (32) but constitute metallic interstitial compounds; as of early 2021, there are only a few computationally predicted perovskite nitrides (33), one of which, $LaWN_3$, was recently synthesized (34). Ternary nitrides can also be viewed from the perspective of shared motifs, such as corner-sharing SiN_4 tetrahedra, which make up nitridosilicates (**Figure 3*d***). These have been considered for applications including phosphors for LEDs (see the sidebar titled Application Spotlight: Phosphors for Solid-State Lighting) (14). Although not discussed in depth here, interstitial ternary nitrides such as the structure shown in **Figure 3*e*** demonstrate metallic behavior as a result of being extremely metal rich and, among other properties, are of interest for ferromagnetic applications (35). Finally, MAX phases and MXenes (**Figure 3*f***) are becoming increasingly common in the literature due to interest in their use for catalysis and for battery applications (see the sidebar titled Application Spotlight: Electrochemical Energy Storage). Ternary nitrides can form in structures beyond those mentioned here, including a range of structures with anion-centered polyhedra [which can be considered antistructures (26)].

2.4. Metastability

In addition to their wide range of structures, nitrides have a higher propensity than other material classes to crystallize in thermodynamically metastable phases, which are crystal structures that are not the thermodynamic ground state. To determine E_{hull}, a compound's free energy referenced to its ground-state energy, many studies use density functional theory (DFT) to calculate

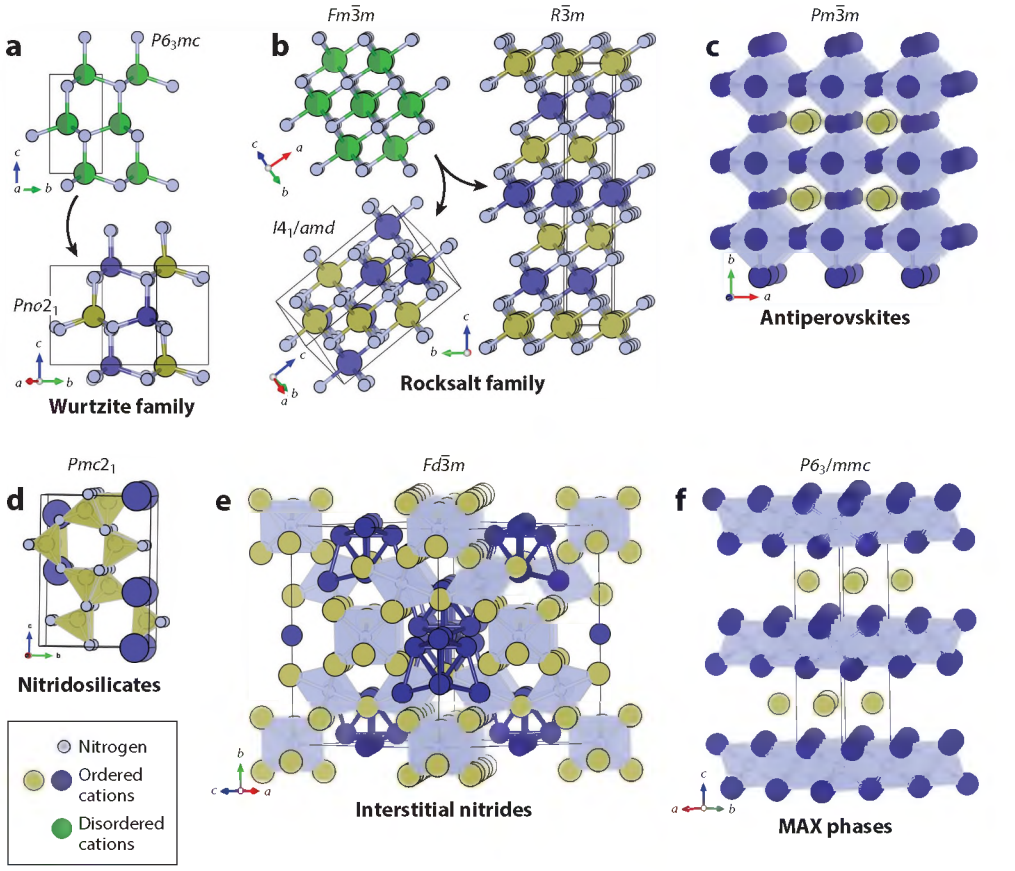

Figure 3

Some structural families of ternary nitrides. Many functional nitrides crystallize in (*a*) polar, tetrahedral wurtzite-derived structures with disordered ($P6_3mc$) or ordered ($Pna2_1$) configurations or (*b*) nonpolar octahedral rocksalt-derived structures with disordered ($Fm\bar{3}m$) and ordered ($I4_1amd$ or $R\bar{3}m$) configurations. (*c*) Antiperovskites in the $Pm\bar{3}m$ structure are also common. (*d*) Nitridosilicates crystallize in myriad structures, many of which are analogous to the large family of silicate oxides. The example shown here is $Sr_2Si_5N_8$ ($Pmc2_1$) owing to its relevance for solid-state lighting phosphors. Also shown are example structures of (*e*) interstitial nitrides and (*f*) MAX/MXene layered structures. All structures are drawn to the same scale.

and compare phase formation energies (38). In DFT databases and high-throughput screenings, E_{hull} (39) is typically estimated by calculating formation energy at 0 K (approximately equal to free enthalpy, H_f), rather than temperature-dependent free energy, G, due to computational simplicity, though doing so neglects entropic effects. In this subsection, reported E_{hull} values refer to relative formation energies calculated by the DFT Generalized Gradient Approximation (GGA), as available on the MP database, unless specified otherwise. Note also that for a given compound to be metastable and synthesizable it must also be dynamically stable (i.e., not have imaginary phonon modes).

To examine metastability and synthesizability, in **Figure 4** we compare the E_{hull} values of predicted and synthesized metastable materials across single-anion compounds in the MP database (see the **Supplemental Material** for details). Although materials with the lowest E_{hull} values tend

APPLICATION SPOTLIGHT: PHOSPHORS FOR SOLID-STATE LIGHTING

Ternary nitrides offer many practical advantages for phosphor and solid-state lighting applications (for a recent review, see 36). To enable luminescence, one typically substitutes in ~1–5% of a lanthanide ion with a partially filled 4f electronic subshell that permits atom-like 4f-to-5d absorption and reemission transitions (e.g., Eu^{2+}). The 5s and 5p orbitals shield the optically accessible 4f subband transitions from lattice coupling, allowing efficient optical absorption and recombination (37). Ternary materials provide an advantage: A stiff main group nitride–based framework (as found in the nitridosilicates; **Figure 3*d***) prevents nonradiative relaxation via phonon quenching, since the relevant phonons have a low population at operation temperatures. The nitrogen-based ligands to the lanthanide provide a larger crystal field splitting with the 5d energy levels than with oxides (e.g., more covalency); thus, the nitride ligand provides a greater ability to tune color, often into the desired red colors. While the quantum efficiencies of the top-performing materials have some room for improvement, the color-rendering index and synthesis remain major challenges.

to be the easiest to synthesize, not all low-energy polymorphs are synthesizable (40). Notably, nitrides have a much larger window of metastable synthesizability than oxides (41), as shown in **Figure 4** by their wide range of E_{hull} values. Metastable oxides, phosphides, and sulfides have quartile E_{hull} values in the range of 0.01 to 0.13 eV/atom for all compounds, while the quartile metastability of both predicted and experimental nitrides extends far higher in energy, from 0.06 to 0.22 eV/atom. Carbides have a lower predicted, but experimentally similar, metastability range than nitrides [the relationship between these two classes varies with temperature (42)]. Note that databases are subject to sampling bias, discussed further in section S1 of the **Supplemental Material**.

Various explanations for thermodynamically metastable phase stability exist in the literature (44). As discussed in Section 2.1, nitrides form mixed ionic–covalent bonds and therefore

APPLICATION SPOTLIGHT: ELECTROCHEMICAL ENERGY STORAGE

Ternary nitrides offer several advantages for battery technologies. α-Li_3N (*P6/mmm*; **Figure 1*a***) was an early candidate material for battery applications due to high Li^+ conductivity arising from intraplanar hopping on lithium vacancies (51). While Li_3N decomposes at ~0.5 V (52), ternaries of the same form ($Li_{3-x}M_xN$; M = Cu, Si, Co, Mn, or Fe) have been explored (52, 53) and show the same propensity for lithium vacancies (54).

These characteristics make ternary nitrides attractive for high-rate, high-capacity electrochemical storage as both electrolytes and negative electrodes (55). Layered compounds allow Li^+ [or other ion (56, 57)] intercalation, and layered $LiMoN_2$ and Li_7MnN_4 (58) have been investigated as electrode materials. Antifluorite (59) and hexagonal lithium nitridosilicates (60) are promising solid-state electrolytes with ion conductivity as high as 5×10^{-2} (·cm)$^{-1}$ at elevated temperatures. In addition, disturbances to the potential landscape of ternary nitrides from cation disorder (**Figure 3**; discussed in Section 3.2) prevent local trapping during ion transport, leading to higher ion conductivity and longer cycle stability (61, 62).

Ternary nitrides have also been suggested as anode coatings, contingent upon low electrical conductivity, high ionic conductivity, and tolerance for cycle-induced strain (55). A primary challenge of nitride electrochemistry is material stability, partially due to the tendency of nitride electrodes to undergo irreversible conversion reactions rather than reversibly intercalating (58). Ternary nitride MAX and MXene phases may also see development for other electrochemical device applications; in particular, nitride MXenes are an emerging focus of intense research (63).

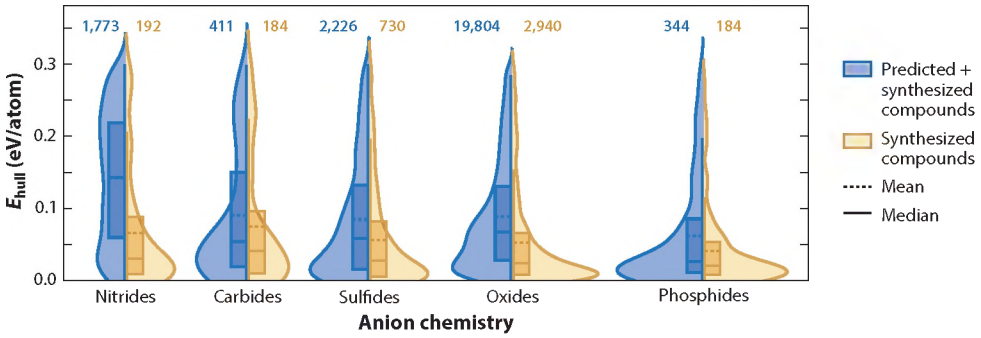

Figure 4

Violin plots comparing metastability across all metastable nitride, carbide, sulfide, oxide, and phosphide compounds in the Materials Project database (43; see the **Supplemental Material** for details). Blue distributions represent all metastable compounds in each class, and yellow distributions represent the experimentally synthesized subset. Box plots describe statistics within each set. Cutoffs correspond to lower and upper quartiles (25% and 75%), solid lines correspond to medians, and dashed lines correspond to means. Numbers above each distribution denote the number of compounds in each class. Further details can be found in section S4 of the **Supplemental Material**.

Energy above the convex hull (E_{hull}): a metric of thermodynamic stability where a convex hull is constructed by connecting the thermodynamic ground-state free energies within its composition phase space. $E_{hull} = 0$ eV/atom, ground state; $E_{hull} > 0$ eV/atom, metastable compound

Chemical potential: the change in free energy upon addition or removal of a component while keeping pressure (p), temperature (T), and other species ($n_{j\neq i}$) constant: $\mu_i = (\partial G/\partial n_i)_{p,T,n_{j\neq i}}$, which leads to its total differential: $d\mu = Vdp - SdT$, where V is volume and S is entropy

compounds with higher cohesive energies, enabling experimental access to higher values of E_{hull} (27). Nitrides (and carbides) also have a significantly higher amorphous thermodynamic upper limits, the energy levels above which compounds cannot be synthesized (45). It is important to consider a compound's metastability with respect to both constituent binaries and competing ternary polymorphs. A ternary nitride can be metastable with respect to its binary nitride endpoints and still be the lowest-energy polymorph at its composition. Metastable polymorphs can also phase-separate and coexist, as recently demonstrated by competing rocksalt- and wurtzite-derived $MgSnN_2$ phases (46). Additional metrics for assessing (meta)stability that are important to consider include "energy above the Pourbaix hull," which accounts for moisture degradation (47, 48).

Metastability is intimately connected to experimental control of the nitrogen chemical potential, μ(N). Synthesis approaches applying a high μ(N) can stabilize metastable phases that would otherwise be outcompeted by binary phase segregation (27, 49) and enable kinetic quenching of metastable phases. Stabilization can also be achieved through defect engineering, alloying, and epitaxial templating (50). Therefore, a primary challenge in nitride synthesis is to maintain (or increase) a high μ(N) through control of experimental parameters. Additionally, the methods used to control μ(N) can greatly influence the defect landscape of a synthesized material. Practical control of μ(N) for a variety of synthesis conditions is discussed further in Section 4.

3. DEFECTS

One of the most challenging yet potentially revolutionary aspects of ternary nitrides is their propensity for complex defects. In this section, we discuss the intrinsic, extrinsic, and extended defects commonly found in ternary nitrides, and the challenges and opportunities posed thereby.

3.1. Intrinsic Defects

Intrinsic defects have historically been pernicious in nitride materials. Though self-interstitials and antisite defects tend to be high energy in binary nitrides, both cation and anion vacancies often cause undesirable compensation of dopants. Cation vacancies become detrimental for wide-bandgap binary nitrides, particularly because defect formation energies typically decrease with

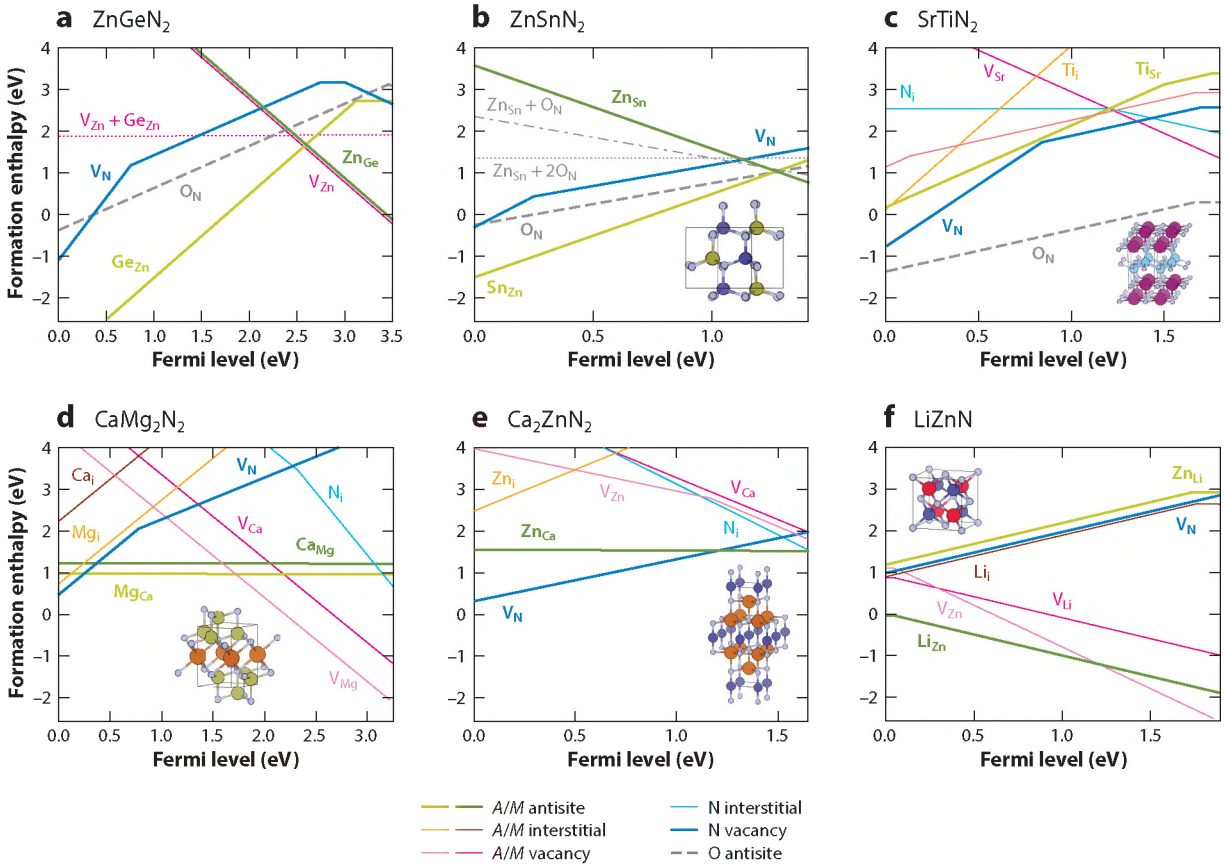

Figure 5

A sampling of defect diagrams, where the Fermi level axis refers to the bandgap, for different inorganic ternary nitrides: (*a*) $ZnGeN_2$, (*b*) $ZnSnN_2$, (*c*) $SrTiN_2$, (*d*) $CaMg_2N_2$, (*e*) Ca_2ZnN_2, and (*f*) LiZnN. Structures are shown in the insets for all materials except $ZnGeN_2$, which is isostructural to $ZnSnN_2$. Further details can be found in section S5 of the **Supplemental Material**. Data in panel *a* from Reference 65. Data in panel *b* from Reference 66. Data in panel *c* from Reference 67. Data in panels *d* and *e* from Reference 18. Data in panel *f* from Reference 68.

increasing bandgap (64). Many of these issues carry over to the ternary nitrides and are made more complex by the sheer number of intrinsic defects enabled by a ternary system.

As computational research on ternary nitrides has increased, defect diagrams have emerged as a way to predict and examine the effects of defects in emerging materials, particularly target compounds for optoelectronic applications. Defect formation energy diagrams visualize the formation energy or enthalpy (E^f) of intrinsic and extrinsic defects as a function of Fermi energy, enabling prediction of defect formation, equilibrium Fermi level, and dopability. A defect's slope indicates its charge, with positive slope indicating an electron donor and negative slope indicating an electron acceptor, and defects with lower E^f are more likely to form. **Figure 5** depicts E^f diagrams for six ternary nitrides spanning a range of structure types. **Figure 5*a*,*b*** shows two *M*–*M*–N compounds, which are wide-bandgap ($ZnGeN_2$) and narrower-bandgap ($ZnSnN_2$) examples of the wurtzite-derived II–IV–N_2 family. $SrTiN_2$, shown in **Figure 5*c***, is an *A*–*M*–N ternary nitride with the same stoichiometry but a layered structure. The materials shown in **Figure 5*d*,*e***, the *A*–*A*–N compound $CaMg_2N_2$ and the *A*–*M*–N compound Ca_2ZnN_2, have cations of the same valence but different

Defect formation energy ($E^f[X^q]$): the energetic cost to create or remove an isolated defect *X* with charge state *q* from a bulk material; defect formation energy calculations are used to assess how likely various defects and dopants are to form compared with one another

stoichiometries than those in **Figure 5*a–c***. Finally, LiZnN, shown in **Figure 5*f***, is an *A*–*M*–N compound where zinc and nitrogen form a zincblende network and lithium occupies tetrahedral interstices. These diagrams are chosen to show chemical potential regimes representative of common synthetic conditions. For example, all the diagrams were calculated in nitrogen-rich regimes, and the cation chemical potentials are chosen to reflect vapor pressure conditions during thin-film, vacuum synthesis (e.g., are zinc-poor). These diagrams represent a variety of bonding configurations, chemistries, and structures but clearly cannot capture defect trends for all ternary nitrides.

Nitrogen vacancies (V_N) are consistently low E^f in ternary nitrides, just as in binaries. As shown in **Figure 5*c–e***, V_N are the lowest-E^f intrinsic donor for $SrTiN_2$, $CaMg_2N_2$, and Ca_2ZnN_2. V_N in $ZnGeN_2$ and $ZnSnN_2$ have similarly low E^f (ranging from −1 eV at the valence band maximum to 3 eV near the Fermi level for $ZnGeN_2$) but are not the lowest-E^f intrinsic donor as a result of more favorable cation antisite defects (discussed further in Section 3.2, below). Similarly, cation vacancies tend to have low E^f in the selected ternary nitrides. In particular, V_{Zn} is the lowest-E^f intrinsic acceptor in $ZnGeN_2$ and has low E^f in Ca_2ZnN_2 and LiZnN, and V_{Mg} has low E^f in $CaMg_2N_2$. Though low-E^f vacancies may negatively affect properties and/or cause undesired defect compensation of extrinsic dopants, they are not always detrimental. For example, lithium vacancies are necessary for ionic charge transport in battery applications (see the sidebar titled Application Spotlight: Electrochemical Energy Storage) (52).

Native antisite defects play a defining role in the defect landscape of ternary nitrides. Antisite defects tend to have higher E^f for ternary nitrides with dissimilar cation atomic sizes such as $SrTiN_2$, in which neither antisite defect has an E^f value below 0 eV (**Figure 5*c***). However, for ternary nitrides where the two cations are close in size, such as wurtzite-derived $ZnGeN_2$ and $ZnSnN_2$ (**Figure 5*a,b***), cation antisite defects such as Zn_{Sn} and Zn_{Ge} have low E^f. The effect of donor doping is to push the Fermi level higher in the bandgap, necessarily decreasing the formation energy of compensating electron acceptors, and the opposite is true for acceptor doping (69). Thus, compensation presents a challenge for applications where extrinsically doped ternary nitrides are desirable. For example, native cation antisite defects are predicted to compensate for $ZnGeN_2$ when doping both n-type (70) and p-type (71). However, it can also be a benefit, for instance, in $ZnSnN_2$, where self-compensation of electron donors with Zn_{Sn} defects enables n-type doping control (72). Similarly, in LiZnN (**Figure 5*f***), the Li_{Zn} antisite is the lowest-E^f defect at energies close to the valence band maximum, indicating that this material is intrinsically p-type (68). There are experimental strategies to prevent defect compensation, including changing μ(N) (73) and codoping with hydrogen or other extrinsic dopants (discussed in Section 3.3). Selection of materials with significant cation size mismatch would result in a greater energetic driving force toward cation order (31), such as in $(Zn,Mg)SiN_2$ compounds compared with $(Zn,Mg)GeN_2$. When antisites are favorable, intentional use of cation off-stoichiometry may offer a route to purely intrinsic bipolar doping. Additionally, in some ternary nitrides, cation antisite defects can form complexes enabling structural tunability, namely the use of cation site disorder as a knob to tune properties.

3.2. Cation Disorder

Cation antisite defect pairs, as discussed above, can be prevalent in ternary nitrides. Antisite defect complexes can exist well beyond the dilute defect approximation typically used in calculations, and at high concentrations are referred to as cation site disorder. Cation-disordered ternary nitrides can be thought of as occurring in higher-symmetry structures with a generic cation site that has partial occupancy for each cation, as shown in **Figure 3*a,b***. This type of disorder

typically (74, 75)—but not always (76)—narrows the bandgap. It is not yet clear what the nature of this modification is—whether a midgap state is introduced that may become band-like at high concentration (77), whether there are near-band-edge "tail" states that effectively narrow the bandgap (78), or whether there is some other mechanism that affects the electronic structure. While its origins are not fully understood, modifying the bandgap through cation disorder is a promising mechanism for bandgap tuning in optoelectronic devices, and cation disorder may affect other properties such as thermal conductivity and ion conductivity (for a recent review, see 79). Remaining challenges to disorder-based tunability include precisely controlling the extent of cation site disorder; accurately characterizing and quantifying disorder; and creating theoretical predictions for realistic, metastable structures.

3.3. Extrinsic Defects

Unintended extrinsic dopants are a major problem for both binary and ternary nitride synthesis. Unintentional oxygen contamination is a crucial issue across all nitrides because of the close atomic sizes of oxygen and nitrogen. Oxygen contamination is difficult to avoid, even in very pure growth environments (64). In group III nitrides, oxygen is a shallow donor and historically caused n-type conductivity in GaN (64). This issue persists in the ternary nitrides (**Figure 5*a*,*c***) (88, 89). If oxygen is present, O_N substitutional defects are low E^f, even at high μ(N). Consequently, oxygen presents a huge challenge to p-type doping of ternary nitrides, and developing synthesis techniques to minimize oxygen incorporation is crucial (88, 90).

In contrast to binary nitrides, oxygen defects can be beneficial in ternary nitrides. O_N substitutional defects can form complexes with acceptors such as cation antisite defects; for example, in $ZnSnN_2$, Zn_{Sn} antisites and O_N defects compensate to create charge-neutral defect complexes, helping to lower the degenerate carrier concentration (91; for more information on $ZnSnN_2$, see 92). Though oxynitride structures are outside of the scope of this review, anion site alloying with oxygen may present opportunities for new structures and properties (89, 93).

Another relevant extrinsic defect is hydrogen, which is often present due to hydrogen-containing nitrogen sources (e.g., NH_3) and can be used to tune the defect landscape in semiconductor materials. Hydrogen (which typically occupies interstitial sites, H_i) tends to suppress the formation of compensating nitrogen vacancies in group III nitrides, and it can then be removed with a postgrowth anneal, thereby activating p-type dopants (64). In this case, the H_i–Mg complex has a lower formation energy than other compensating defects, allowing compensation to occur without occupation of a lattice site. In turn, H_i is easily removed with a postgrowth anneal, activating the magnesium. The same effect has been demonstrated in ternary nitrides: Growth in a hydrogen environment followed by a postdeposition anneal has been shown to passivate acceptors in $ZnSnN_2$ (94) and has been theorized to do the same in $ZnGeN_2$, but hydrogen passivation is an open area of research in other ternary nitrides (71). While intentional extrinsic doping of ternary nitrides will be critical for their use in some applications, this research has largely been limited to computational work (67, 70, 71). Experimental investigation of such dopants is currently an underexplored area of research.

3.4. Extended Defects

As discussed in Section 2.4, metastable polymorphs are prevalent in nitrides. The zincblende polymorph of GaN lies only a few meV above the wurtzite ground state (95), leading to prevalent inclusions of zincblende in normally wurtzite material, or stacking faults. For ternary nitrides, the presence of another cation increases polymorph diversity, allowing for multiple cation-ordered polytypes within the same structural family and for polymorphs of entirely different

structure types. Like other II–IV–N_2 family compounds, $MgSnN_2$ forms in a wurtzite-derived orthorhombic structure. Here, the orthorhombic unit cell is a $2\times\ 2\ \times 1$ supercell of wurtzite cells with a slight bond distortion from the heterovalent cations. One cation site swap per unit cell produces two antisite defects, but two cation site-swap actions produce a different space group—changing from $Pna2_1$ to $Pmc2_1$. An inclusion of one space group within another can be thought of as a stacking fault, but one that retains the wurtzite-derived structure rather than a cubic (zincblende) inclusion. The effect of this type of stacking fault is predicted to be electronically benign as long as the local octet rule is satisfied (78, 96). The energy difference between the two wurtzite-derived space groups for $MgSnN_2$ is only 5 meV/atom, and two similarly related zincblende structures lie 25–30 meV/atom above the ground state, suggesting that stacking faults similar to GaN may occur in this material. However, to date, only wurtzite-type and substantially more metastable rocksalt $MgSnN_2$ (70–100 meV/atom) have been observed (46, 97); the coincident formation of these polymorphs likely results in similar extended defects to stacking faults. In addition, there may be inhomogeneous regions of more or less cation-disordered phases, which could result in potential fluctuations.

4. SYNTHESIS OF TERNARY NITRIDES

The synthesis of ternary nitride materials revolves around the challenge of maintaining a high μ(N) while also enabling mass transport and crystal growth. We begin this section with an overview of μ(N) and then discuss synthetic methods according to the dominant method of controlling μ(N): Bulk processes are classified by control via pressure, while thin-film processes are classified by deposition chemistry. Despite the differences between μ(N) control in bulk and thin-film methods, there are cross-cutting challenges for the synthesis of ternary nitrides across these techniques. In addition to the discussion of μ(N) presented here, several other reviews discuss synthesis techniques of ternary nitrides in greater detail (26, 98).

4.1. Controlling Nitrogen Chemical Potential

Figure 6*a* highlights how the synthesis of ternary nitrides is sensitive to μ(N), as shown for the magnesium- and zinc-based ternary nitrides. The conditions used to determine stability in **Figure 6*a*** are explicitly connected to common synthetic conditions in **Figure 6*b***. With open systems, increasing temperature decreases μ(N); as such, one may employ lower temperatures by using more aggressive chemical reactants (e.g., NH_3, N_2H_4) in order to retain a high effective chemical potential while promoting chemical reactivity. While atmospheres of NH_3 and N_2H_4 have enhanced reactivity relative to N_2, they do not have an elevated μ(N) according to the rigorous definition shown in the margin due to their equilibrium decomposition at elevated temperature to N_2 and H_2 (100). Regardless, these species are more kinetically active (e.g., due to their lack of triple-bonded nitrogen) and can yield thermodynamically spontaneous reactions due to the formation of H_2 or H_2O as by-products. In contrast to open systems, closed systems generate elevated μ(N) through the use of pressure. Vacuum chambers permit additional modification of μ(N) on the basis of their ability to generate various nitrogen-based plasmas. Plasmas can contain a mixture of atomic nitrogen species or metastable excited molecules with an elevated μ(N) (101), and their composition can have a significant influence on growth rate (102), surface morphology, and defect concentration (103). As an additional point of comparison, O_2 has a lower chemical potential compared with N_2 at standard conditions: $\mu(O_2) = -0.318$ eV/atom versus $\mu(N_2) = -0.298$ eV/atom (99). Oxides are more stable versus O_2 than nitrides are versus N_2, H_f(0K): Si_3N_4 −1.3 eV/atom versus SiO_2 −3.3 eV/atom (43), when referencing gases in their standard state.

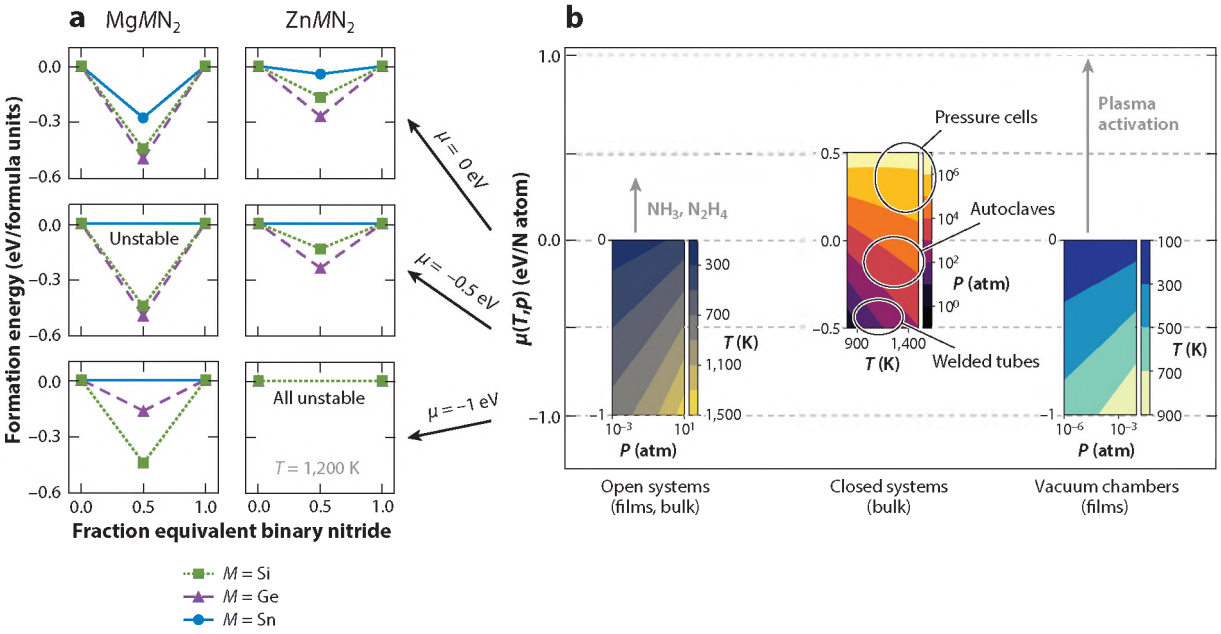

Figure 6

(*a*) Thermodynamic convex hull constructions using Gibbs free energy illustrate how shifting μ(N) changes the stability of MgMN$_2$ and ZnMN$_2$ compounds (M = Si, Ge, and Sn). Colors correspond to M species. All calculations were run at T = 1,200 K for (*top*) μ = 0 eV/atom, (*middle*) −0.5 eV/atom, and (*bottom*) −1.0 eV/atom. Values were calculated using the Gibbs predictor in a Grand Potential (42, 104). Elevated μ(N) is required to stabilize ZnMN$_2$ compounds compared with MgMN$_2$ for a given M cation. (*b*) Approximate mapping of synthesis methods onto the chemical potential of nitrogen with respect to standard conditions, $\mu(T,p) = \mu(T,p_0) + kT \ln(p/p_0)$, where $p_0 = 10^5$ Pa or 1 bar and assuming ideal gas behavior: open systems, closed systems at elevated pressure, and closed systems at low pressure (vacuum systems). Use of NH_3 or N_2H_4 can result in a higher effective chemical potential if one assumes that atomic nitrogen rather than N_2 is produced (27). In the synthesis of thin films [or in some bulk reactions (105)], a plasma discharge can increase the effective chemical potential by nearly ∼1 eV/atom (106). Across these synthetic regimes, μ(N) is tunable by >2 eV/atom. Further details can be found in section S6 of the **Supplemental Material**.

4.2. Bulk Synthesis and Crystal Growth

As shown in **Figure 1*a***, the earliest demonstrations of ternary nitride materials relied on bulk synthesis (4), and these techniques have continued to play a major role in the development of this class. Bulk syntheses enable materials discovery with the ability to control crystallization and cation ordering, which may not be available in thin-film geometries. Bulk processes are useful for synthesizing powder and single-crystalline materials in order to investigate their crystal structures and basic optical, thermodynamic, and magnetic properties. We classify bulk syntheses either as being in an open system, which has a practically infinite reservoir of nitrogen at a constant μ(N), or as being in a closed system, which has a finite amount of nitrogen such that μ(N) may evolve over the course of a reaction.

4.2.1. Open systems, ambient pressure. Synthesis with open chemical systems often relies on the gas-phase nitridation of precursor materials with a range of nitrogen sources. For electropositive s-block, lanthanide, or early transition metals, N_2 is sufficiently oxidizing to support nitride formation, as in the synthesis of LnSi$_3$N$_5$ (Ln = lanthanide) from biphasic lanthanide–silicon alloys (14) or MgMoN$_2$ from the reaction of N_2 with Mg_3N_2 and molybdenum (56).

Others include LiMgN (59); $Li_2Zr_2N_2$ and Li_2HfN_2 (107); Ca_2TiN_4 and Ca_5NbN_5 (108); Li_7MnN_4 (109); $MgTa_2N_3$, $Mg_2Ta_2N_4$, and $CaTaN_2$ (57); and $ScTaN_2$ (110). Other solid-state reactions, such as direct reaction of the binary nitrides, can proceed under N_2 atmosphere at high temperature if the formed compound is sufficiently stable to overcome the reduced μ(N) at elevated temperature, such as the production of $MgSiN_2$ from its constituent binaries (111). Some reactions are even robust enough to proceed in ambient atmospheres with the right precursors, such as the flame-propagated synthesis of $MgSiN_2$ from the metathesis of Mg_3N_2 and SiO_2 (112), although with oxygen inclusion in the product.

Ammonolysis reactions based on traditional solid-state chemistry, although they require temperatures >900°C, are convenient for the atomic-scale mixing of metals within a ternary oxide host, as in the reaction $Zn_2GeO_4 + 3NH_3 \rightarrow ZnGeN_2 + Zn(g) + 4H_2O(g) + \frac{1}{2}N_2(g) + \frac{1}{2}H_2(g)$ (113), or for the production of $LiMoN_2$ from Li_2MoO_4 (114). NH_3 serves as a reactive, activated nitrogen source but, in contrast to N_2, is fairly reducing from the equilibrium decomposition of NH_3 into N_2 and H_2. Creative gas plumbing has been used to delay ammonia decomposition at high temperature by keeping the gas cool before contacting the solid powders (115). While the reaction of oxides in ammonolysis yields an additional thermodynamic benefit from producing $H_2O(g)$ as a side product, the incorporation of oxygen in the final product is a substantial concern (see Section 3.3); however, ammonolysis is not limited to oxides as source material (116).

Reactive nitrogen–containing precursors in open systems backed with near-ambient partial pressures of N_2 and NH_3 maintain a sufficient μ(N) to drive synthesis of nitrides. Silicon diimide [$Si(NH)_2$], an industrial precursor of Si_3N_4, can be reacted directly with alkaline earth or lanthanide metals at temperatures in excess of 1,500°C to form very stable phases such as $CeSi_3N_5$ (14, 117). Likewise, metal amides serve to increase reactivity, as found in the production of Na_3WN_3 from W_2N with excess $NaNH_2$ (118). However, in all cases with open systems, it remains difficult to react the more electronegative metals (e.g., tin) or avoid the inclusion of oxygen-based impurities without special purification procedures.

4.2.2. Closed systems, elevated pressure. Closed systems are especially appropriate for reactions of binary nitrides, where all nitrogen needed for the final product is embedded in the precursor materials. These reactions are well suited for ternaries where one or more metal is an alkali or alkaline earth metal due to the availability of nitrogen-containing precursors [e.g., Li_3N, Mg_3N_2, Sr_2N, and Ca_3N_2 (56, 59, 108)], and can be extended to NaN_3-based compounds with appropriate safety precautions for azide use (see the sidebar titled Safety). Reactions of binary nitrides are typically contained in welded, refractory metal tubes to avoid reaction of the metals with other containers (e.g., as occurs with SiO_2) and to retain a reasonable μ(N) for the endogenously released nitrogen. However, for lower-temperature reactions ($T < 1{,}000$ K), ion-exchange or double-exchange reactions can take place in an inert-atmosphere glove box (119, 120) or an evacuated SiO_2 ampoule (121).

SAFETY

All synthetic routes described here present their own hazards, but many are more hazardous than might be expected given the benign nature of nitrogen itself. Inorganic azides (N_3^-) are acutely toxic and extremely hazardous, especially because they are prone to decomposition by release of N_2. Supercritical NH_3 is accessible above 405 K/132°C and 11.3 MPa/110 bar, requiring special considerations for such high temperature and pressure. Carcinogenic N_2H_4, which can be a nitrogen source for bulk and thin-film syntheses, decomposes spontaneously in the presence of many metal catalysts, including some of the metals identified in **Figure 1*b***.

Welded tubes are also used for reactions performed in molten, metallic fluxes and have found success in crystal growth and materials discovery efforts. The molten metal serves not only to enhance mass transport but also to increase μ(N) by dissociation of N_2 into the metal, creating an activated species. These methods have been employed for GaN synthesis, where use of sodium flux rather than gallium self-flux reduces the needed pressure from $\sim 10^4$ atm of pressure at 1,500°C (122) to 50 atm of N_2 at 750°C (123). Specific to the synthesis of ternary nitrides with alkaline earth metals, inclusion of calcium, strontium, and barium in molten sodium can increase the solubility of nitrogen to ~1.1 mol%, attributable to the formation of species such as [Ba_4N] (124, 125). The use of alkali or alkaline earth metal fluxes (including eutectic mixtures) (125) has led to the growth of Ba_2ZnN_2 and Sr_2ZnN_2 (126); $Ba_3Ga_2N_4$, $Ba_5Si_2N_6$, and $Ba_3Ge_2N_2$ (127); and $Ca_6Te_3N_2$ (128), as well as higher-order multinary nitrides.

4.2.3. Closed systems, extreme pressure. A powerful approach in the discovery and crystal growth of ternary nitrides involves ammonothermal reactions held in specially designed autoclaves. Through the use of corrosion- and high-temperature-resistant alloys (e.g., nickel-based superalloys), reactions can be conducted in supercritical NH_3 at high temperatures (>600°C) and pressures (>600 MPa or 6 kbar) (129–131). The high-mobility, high-μ(N) supercritical fluid provides an ideal environment for synthesis, and the solution chemistry can be carefully tuned using various mineralizers (e.g., acidic, NH_4X; basic, ANH_2). This tuning is vital for the successful formation of ternary nitrides (130) and can be used to enable or suppress intermediate species or defects (e.g., mixed-metal amides and hydride formation, respectively). The supercritical ammonia approach has been used with the basic mineralizer KNH_2 to synthesize $ZnSiN_2$ and $ZnGeN_2$, with strong evidence of cation ordering at $T = 870$–$1{,}070$ K and $P \leq 230$ MPa or 2.3 kbar (132). These methods are ideally suited for fundamental studies that require high-quality single crystals, as well as exploratory synthesis, and are reviewed in depth elsewhere (131). However, the expense and expertise required to mitigate hazards of these processes have prevented widespread adoption.

Multi-anvil presses, while also specialized and expensive, feature fewer hazards. μ(N) is high above gigapascal-scale hydrostatic pressures at $T > 1{,}000$ K [$\mu - \mu(T_0, p_0) > 0$ eV/atom (**Figure 6*b***)], and extreme temperature and pressure also increase the (normally prohibitively slow) solid-state diffusion (133) needed for the crystallization and cation ordering of many ternary nitrides (18, 134). For instance, while the metathesis reaction among $ZnCl_2$, Si_3N_4, and LiN_3 in a welded tantalum tube at 700°C yields nanosized grains of $Pna2_1$ $ZnSiN_2$ with cation ordering, annealing at 6 GPa and 1,200°C is required for full crystallization of the material (134). In some cases, a judicious choice of precursor is required to ensure atomic-scale mixing of the reaction, as in the metathesis of fluoride salt precursors to crystallize $ZnSnN_2$ at 5 GPa (135). The low throughput and significant expense of extreme pressure reactions have reserved their use for specialized, basic science studies.

4.3. Thin-Film Synthesis

The requirement for thin-film geometries in many device applications has led to the widespread use of physical and chemical vapor deposition (PVD and CVD) techniques and an increasing role for these techniques in materials discovery. Thin-film synthetic methods have simplified the measurement of certain properties, such as electronic transport and optical phenomena, which are difficult to directly probe using bulk material and are crucial for many device applications. While we divide techniques between common PVD and CVD types, many thin-film growth methods do not fall neatly into either category (136–139). Additional discussion of these techniques can be found in Reference 98.

4.3.1. Physical vapor deposition. PVD methods including reactive sputtering and plasma-assisted molecular beam epitaxy (MBE) have been extremely useful for the discovery of ternary nitrides. The success of these techniques derives mainly from the use of plasma nitrogen sources, which adds another variable besides temperature and pressure to μ(N) (**Figure 6*b***). Note that modeling and predicting the resulting μ depend on various and complex factors pertaining to the plasma (see the **Supplemental Material**). The plasma composition strongly influences the properties of the deposited material, in both phase selection and defect formation. Plasma activation may be necessary to stabilize some materials (**Figure 6**). However, high-ion-content plasma (e.g., electron cyclotron resonance) can increase defect density in films through impact damage when ions are accelerated by an induced floating potential (103), and increased ion concentration in the plasma can lead to higher defect concentrations and poor optical properties (140, 141). Materials with lower bond strength (comparatively lower bandgaps), such as $ZnSnN_2$, are more susceptible to plasma damage. In sputtering, accelerated ions in the plasma are necessary to knock source atoms from the targets. Accelerating potentials in sputtering are often much higher than in MBE, causing ions to bombard the growing surface with up to 40 eV of kinetic energy (142). Various methods can be used to decrease ion damage in sputtering, such as increasing operating pressure (increasing gas-phase collisions) or using decelerating substrate potentials, pulsed high-frequency signals (143), and off-axis geometries (144). In other cases, ion bombardment can provide beneficial energy for crystallization and enhancement of gas reactivity (145).

A major benefit of PVD methods is the relative simplicity of the techniques and precursors, which enables rapid mapping of thin-film deposition space through combinatorial synthesis. Rapid screening of deposition conditions (e.g., metal flux, temperature) onto a stationary substrate with intentionally nonuniform temperature effectively enables many deposition experiments to occur at the same time. While this approach is most often used in reactive sputtering, it has also been demonstrated for other PVD and some CVD techniques (146). Although combinatorial approaches are sometimes considered to produce lower-quality material (due to high deposition rates and varying composition), some recent research has demonstrated heteroepitaxy (46, 89), suggesting that this approach can be used to identify conditions appropriate for high-quality thin-film growth as well as materials characteristics.

The ease of obtaining activated N_2 via plasma in PVD methods and the lack of competing side reactions have facilitated demonstrations of new ternary nitrides. However, avoiding plasmas in PVD is also possible, for example, using ammonia MBE; the trade-off is that high substrate temperatures are required to crack NH_3. This high-temperature cracking requirement can conflict with the need to deposit many ternary nitrides at low temperature, driven by the desorption of high-vapor-pressure elemental sources (e.g., zinc and alkali or alkaline earth metals) (46, 147). Zinc-containing compounds such as $ZnGeN_2$, $ZnSnN_2$, and $CaZn_2N_2$ must be deposited below 500°C in order to prevent zinc desorption (17, 65, 72, 88, 148). Higher temperatures would be beneficial to improve film morphology and crystallinity, as well as to reduce defect concentrations.

4.3.2. Chemical vapor deposition. In contrast to PVD, CVD methods rely on the high activity and reactivity of gas-phase precursors and gas-phase thermodynamic by-products [e.g., hydrocarbons, H_2(g) and HCl(g)] to yield nitride product formation. A major benefit of this approach is the larger pressure and temperature windows for deposition afforded by the ability to choose appropriate precursors and supply them in the gas phase. Here, μ(N) is indirectly controlled by the reactivity of the nitrogen-containing source, which may be N_2 plasma or NH_3, or, less commonly, N_2 or N_2H_4 (149, 150). In metal–organic chemical vapor deposition (MOCVD, also called metal–organic vapor-phase epitaxy), additional control is available in the form of various metal–organic sources. For instance, $ZnGeN_2$ has been grown by MOCVD through the use of diethyl zinc with

NH_3 and GeH_4 (87, 151), as well as with remote nitrogen plasma and $Ge(CH)H_3$ (152). Although MOCVD and the related process hydride vapor-phase epitaxy are prominent growth methods for thin films of group III nitride binaries and alloys, there are very few reports of other ternary nitrides synthesized by these methods, with the above examples and a lone report of hydride vapor-phase epitaxy of polycrystalline $ZnGeN_2$ from metallic sources and N_2 (153). If suitable precursors can be identified for metals in a given ternary nitride, these techniques can likely be adapted to afford the high-quality growth of thin films of such materials. For exploratory synthesis, however, precursor cost and safety hazards present a substantial barrier to entry, particularly for MOCVD.

4.4. Integration with Binary Compounds

As discussed throughout this review, ternary nitrides often have structures derived from binaries, which can enable heteroepitaxial integration. For example, wurtzite-derived ternaries can be used as active layers in devices to expand the application space of binary group III nitride compounds. Opportunities include the use of ternary nitride emitter layers in LEDs (see the sidebar titled Application Spotlight: Optoelectronic Devices), hybrid high-electron-mobility transistor devices (see the sidebar titled Application Spotlight: Ultrawide-Bandgap Electronic Devices), contact layers, photovoltaic absorber layers, lower-cost substrates, cladding layers with different refractive indices, and more. Most heteroepitaxy research to date has focused on known systems with zinc or magnesium cations: $ZnSnN_2$ (148), $ZnGeN_2$, and $MgSnN_2$ have all been integrated with GaN, as shown in **Figure 7*b*,*c*** (17, 46, 87). However, there is a huge opportunity space for development of new materials.

APPLICATION SPOTLIGHT: OPTOELECTRONIC DEVICES

A promising application for ternary nitrides is in the active regions of light-emitting devices and solar cells. For example, proposed LED device architectures utilize $ZnGeN_2$ and GaN to achieve longer-wavelength light emission (80, 81), and there is a preliminary demonstration (16) of $ZnSnN_2$ as a thin-film photovoltaic material composed of Earth-abundant elements (72).

Because cation antisite defects are prevalent in ternary nitrides, their impact must be considered for devices where recombination and minority carrier lifetimes are critical (77, 78). Defects can lead to nonradiative recombination pathways through trap-assisted recombination, but localization and energy of the trap state are important in determining recombination lifetimes. Localized defect states result in lattice distortions, increasing the probability of phonon-mediated recombination (82). In contrast, band-like defect states suppress trap-assisted nonradiative recombination (83, 84).

Defects become band-like when their concentration exceeds the Mott threshold (85); antisite defects could potentially form as complexes in cation-disordered (high-concentration) cases, suppressing trap-assisted nonradiative recombination [assuming that band-like states will form deep within the bandgap, based on experimental midgap cathodoluminesence in $ZnGeN_2$ (77)]. Some defect complexes are uncharged (zero slope in a defect diagram), and the energy at which they charge may not lie in the bandgap (e.g., the V_{Zn}–GeZn complex; **Figure 3*a***); such energetically favorable intrinsic defects should also be considered.

Cation-disorder-induced bandgap narrowing, if controllable, can be a powerful tool for optical device engineering, potentially enabling LEDs with disordered quantum wells and ordered barriers of the same composition, or low-cost photovoltaic devices with disorder-tunable bandgaps (79, 86). Integration of bandgap-tunable ternary nitrides with mature systems like GaN, as discussed in Section 4.4, would allow layers to be chosen for optimal optical function without regard to dopability, relying on the mature system for carrier injection (17, 79, 87).

APPLICATION SPOTLIGHT: ULTRAWIDE-BANDGAP ELECTRONIC DEVICES

Wide-bandgap semiconductors form the basis of emerging power electronic devices; the bandgap energy informs the critical field for dielectric breakdown (*EC*) that drives figures of merit for high-power devices (156, 157). Nitrides are of interest because of their high mobilities, ultrawide bandgaps (UWBGs; >3.4 eV), and polarization, enabling high-electron-mobility transistors (HEMTs). Many UWBG ternary nitrides (**Figure 7*a***) may be integrable with known materials.

The polarization properties of wurtzite-based ternary nitrides are interesting in conjunction with traditional alloys or binary nitrides. The recently proposed $ZnSiN_2$/AlN polarization-induced HEMT has a nearly lattice-matched interface with a large polarization discontinuity (158) that induces an electric field, accumulating carriers into a nominally undoped channel with extremely high mobility. Such a device could outperform current AlGaN/GaN HEMTs. Some UWBG ternary nitride device architectures may be limited by their dopability: Ternaries with low-enthalpy antisite defects will likely exacerbate self-compensation of extrinsic dopants (Section 3). However, some device architectures may not rely on doping control in the ternary nitride (see Section 4.4).

Wurtzite AlScN has found success as a piezoelectric material (159) and has recently demonstrated ferroelectric switching (160). This experimental performance, combined with its compatibility with existing materials, indicates great promise for polarization-based applications. A family of distorted perovskite nitrides has also been predicted to show ferroelectric behavior, with polarity modifiable by an applied electric field (33). The ferroelectric perovskite ternary nitride LaWN3 was recently experimentally demonstrated (34). The addition of ferroelectric (and magnetic) materials to the ternary nitride material property landscape will allow the fabrication of devices with new and useful applications (161).

The starting point for exploring materials for integration with binaries is to consider the M_x–M_y^{G+}–N_z space, where G is the oxidation state of the second metal M. These materials tend to be either wurtzite-derived or rocksalt-derived structures. **Figure 7** maps the bandgaps and hexagonal lattice constants of some promising ternary nitride compounds, along with relevant binary compounds. DFT formation enthalpy calculations using the E_{hull} formalism were used to determine if the thermodynamic ground state is rocksalt or wurtzite derived, and GW-calculated bandgaps maintaining the GGA(+U) wave function are reported (154). Heteroepitaxial integration can potentially occur along a vertical line with finite width (within an approximately 1% lattice constant). Not shown in the figure are many promising materials that have been predicted but not yet experimentally reported. For example, $MnSnN_2$, $LiVN_2$, and $CaSnN_2$ are in MP and may form in wurtzite-derived structures compatible with group III nitrides.

Synthesis challenges in realizing these heterostructures include symmetry differences of ordered and disordered ternaries, volatility, and reactivity. When nucleating a lower-symmetry structure (ordered ternary) on a higher-symmetry one (binary or disordered ternary), there are two translationally equivalent possible nucleations, leading to threading dislocations at grain boundaries (155). Nucleating high symmetry onto low symmetry generally does not lead to additional extended defects. In addition, many of the cations constituting ternary nitrides are highly volatile, which may limit growth temperatures and the ability to overgrow ternary layers with binaries. Finally, some of the cations may be reactive with oxygen, constraining growth methods.

4.5. Challenges and Promise in Ternary Nitride Synthesis

Because the synthesis of ternary nitrides is a relatively young field, there remain substantial challenges to its development. As depicted in **Figure 6**, established synthesis methods span a range of μ(N) values; however, increasing temperature, which is needed for mass transport in bulk methods

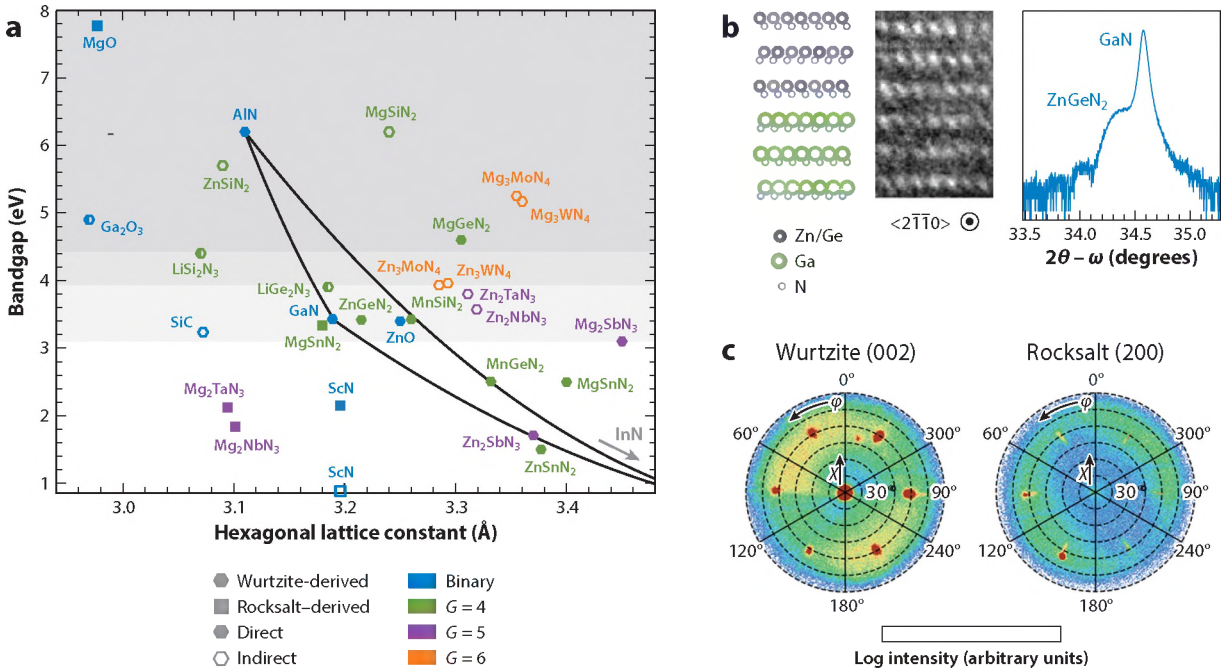

Figure 7

(*a*) Bandgaps and lattice constants of selected wide-bandgap rocksalt- and wurtzite-derived ternary nitrides, where *G* is the oxidation state of the second cation, along with selected binary compounds from the same range. Demonstrations of binary nitride/ternary nitride heteroepitaxial integration have been experimentally demonstrated in a few compounds, including (*b*) $ZnGeN_2$ and (*c*) $MgSnN_2$. Half-shaded data points represent materials with similar computed direct and indirect transitions. Further details can be found in section S7 of the **Supplemental Material**. (*b*) A crystallographic model and corresponding high-resolution scanning transmission electron microscope image of a $ZnGeN_2$/GaN heterointerface, along with X-ray diffraction demonstrating a smooth surface and interface through coherent thickness fringes (17). (*c*) XRD pole figures of $MgSnN_2$ sputtered on GaN. The pole figures are taken along the wurtzite-derived (002) scattering plane and the rocksalt-derived (200) scattering plane, showing the stabilization of both phases (46). Panel *b* adapted with permission from Reference 17, copyright 2020 American Chemical Society. Panel *c* adapted with permission from Reference 46, copyright 2020 American Chemical Society.

and to improve material morphology and crystallinity in thin-film methods, universally decreases μ(N). New, innovative approaches to maintaining a high (effective) μ(N) and/or supporting nitrogen reactivity at lower temperature should gain significant traction in the future. As highlighted throughout this section and our discussion of defects, oxygen incorporation in particular is problematic in both bulk and thin-film ternary nitride synthesis, but many reports of new materials do not adequately control or even document the presence of oxygen. As discussed above, some bulk synthesis methods result in oxygen incorporation from the precursors; oxygen incorporation from deposition chamber components or contaminated sources is pernicious in thin-film methods, and thin films are also prone to postgrowth oxidation. Together, these issues should be a major focus of development for both bulk and thin-film synthetic methods in the future.

Where there are challenges, there is also opportunity, and we therefore describe some areas of development for ternary nitride synthesis. One is a trend toward bulk synthesis without control of μ(N) using pressure. Given the importance of μ(N) in controlling nitride formation, various approaches are gaining traction in basic research, such as the use of reactive fluxes and metathesis [e.g., carbodiimides (162, 163) and amides (164)], as well as the use of reactive gases outside traditional thin-film deposition chambers [e.g., N_2H_4-based atomic layer deposition

(165) or N_2-based plasma (12, 166)]. Another is the specific selection of substrates in order to stabilize metastable phases during deposition, an exciting possibility given the opportunities for heteroepitaxial integration discussed above. This approach has already proven successful for alloys of AlN and ScN (167).

5. CONCLUSIONS

Ternary nitrides have been steadily gaining interest as new compounds with compelling properties are predicted and synthesized. In particular, the pace of predictions has accelerated, meaning that many interesting compounds have yet to be experimentally realized. This array of possibilities stems from the diversity of nitride chemistry, including the ability of nitrogen to form bonds ranging from covalent to ionic and to support many coordination numbers, factors that give rise to a breadth of ternary nitride structures and properties. Many of these materials are metastable yet synthesizable, since their metastability often reflects the stability of N_2 as a decomposition product.

Defects both limit and enable device applications for ternary nitrides. As with binaries, ternaries have low-energy nitrogen vacancies, which can be problematic in light of the difficulty in enhancing nitrogen reactivity in synthesis. Compounding this issue is the favorability of oxygen replacement of nitrogen, leading to pernicious unintentional oxygen incorporation. Cation antisite defects and vacancies are also favorable and can have positive or negative consequences, depending on the desired properties. Cation site disorder may be useful as a method for tuning properties if it can be properly controlled and characterized, and cation vacancies can enable ion transport for applications such as batteries. However, cation site flexibility can limit doping control, as many of these materials self-compensate.

A major challenge facing ternary nitride materials discovery and application development is the difficulty of synthesizing high-quality material due to the extreme stability of N_2. Many synthesis techniques have been developed to address this issue, particularly the use of active nitrogen such as plasma sources, ammonia, hydrazine, or other reactive nitrogen–containing materials that react much more easily to form desired compounds. Temperature and pressure also provide effective knobs for tuning deposition methods; in particular, ternary nitrides benefit from extremely high-pressure synthesis methods similar to those used for more traditional binary nitrides. Both thin-film and bulk deposition techniques, including high-throughput methods such as combinatorial film growth, have been developed to address the need for exploratory synthesis in this relatively new field.

Several crucial advances are needed as ternary nitrides are further explored. New high-throughput synthetic methods should be developed to allow control of a wide range of cation precursors while maintaining high μ(N) in order for experiments to keep pace with computational predictions of new materials. Highly reactive, but very pure, precursors are needed for both bulk and thin-film growth methods to reduce oxygen incorporation while facilitating synthesis of metastable ternaries. High-quality syntheses should be pursued to enable true property interrogation; to that end, methods that enable characterization of antisite defects and cation disorder across length scales and in multiple material forms (powders, single crystals, thin films) are needed to provide feedback to synthesis. Such methods should ultimately enable control of intrinsic doping by cation stoichiometry and low-defect-density ternaries, especially if antisite defect formation is to be suppressed. Finally, the development of new substrates that can enable high-quality epitaxial growth of ternary nitrides and even provide phase stabilization will be needed in order to achieve the potential of these materials across device applications.

Although ternary nitrides are a fairly new class of materials, promising applications have already emerged. Phosphors for solid-state lighting have been developed on the basis of nitridosilicates,

where the stiff framework limits phonon-related losses. The existence of lithium-based ternary nitrides has spurred interest in these materials for battery applications, even beyond lithium ions. The existence of many ternary nitrides with ultrawide bandgaps (>3.4 eV) and polar crystal structures means that ternary nitrides have great potential for electronic devices such as high-frequency and high-power electronics; however, difficulties related to doping may prove challenging or insurmountable due to self-compensation. Optoelectronic applications are also fertile application spaces for ternary nitrides, and devices such as Earth-abundant photovoltaics and visible-spectrum LEDs currently motivate research in this field. For light-emitting and electronics applications in particular, the ability to form heterostructures with group III nitride materials may ease the path toward implementation of ternary nitrides by alleviating practical concerns such as doping and forming electrical contacts. While some of these applications are still in their conceptual stages, predictions have motivated increasing research toward device applications.

DISCLOSURE STATEMENT

A.C.T. has submitted US Patent Applications for a ternary nitride negative electrode–based lithium-ion battery (16/983,672) and $Zn(GeSn)N_2$ for green-amber LEDs (16/941,949). The authors are not aware of any affiliations, memberships, funding, or financial holdings that might be perceived as affecting the objectivity of this review.

ACKNOWLEDGMENTS

Primary support for the writing of this review was provided by the US Department of Energy (DOE), Office of Science, Basic Energy Sciences, Materials Sciences and Engineering Division. This review was authored in part by the National Renewable Energy Laboratory (NREL), operated by Alliance for Sustainable Energy, LLC, for the DOE under contract DE-AC36-08GO28308. A.L.G. acknowledges support from the Director's Fellowship within NREL's Laboratory-Directed Research and Development program. R.W.-R. acknowledges support from the UC Berkeley Chancellor's Fellowship and the National Science Foundation (NSF) Graduate Research Fellowship under grants DGE1106400 and DGE175814. J.R.N. thanks Matt McDermott for insightful discussions and acknowledges funding from the NSF under grant DMR-1653863 and a Sloan Research Fellowship from the Alfred P. Sloan Foundation. E.S.T. was supported by the NSF under grant DMR-1555340. The authors thank Vanessa Meschke for assistance with the periodic table in **Figure 1**.

LITERATURE CITED

1. Zhang Y, Zindler A. 1993. Distribution and evolution of carbon and nitrogen in Earth. *Earth Planet. Sci. Lett.* 117:331–45
2. Zakutayev A. 2016. Design of nitride semiconductors for solar energy conversion. *J. Mater. Chem. A* 4:6742–54
3. Sun W, Bartel CJ, Arca E, Bauers SR, Matthews B, et al. 2019. A map of the inorganic ternary metal nitrides. *Nat. Mater.* 18:732–39
4. Juza R, Hund F. 1946. Die Kristallstrukturen LiMgN, LiZnN, Li_3AlN_2 und Li_3GaN_2. *Naturwissenschaften* 33:121–22
5. Wintenberger M, Maunaye M, Laurent Y. 1973. Groupe spatial et ordre des atomes de zinc et de germanium dans $ZnGeN_2$. *Mater. Res. Bull.* 8:1049–53
6. Patterson FK, Ward R. 1966. The preparation and properties of some ternary nitrides of strontium and barium with rhenium and osmium. *Inorg. Chem.* 5:1312–16

7. DiSalvo FJ, Clarke SJ. 1996. Ternary nitrides: a rapidly growing class of new materials. *Curr. Opin. Solid State Mater. Sci.* 1:241–49
8. Brese NE, O'Keeffe M. 1992. Crystal structure of inorganic nitrides. In *Complexes, Clusters, and Crystal Chemistry*, pp. 307–78. Berlin/Heidelberg: Springer. Struct. Bond. Vol. 79
9. Fitzmaurice JC, Hector AL, Parkin IP. 1993. Low-temperature routes to early transition-metal nitrides. *J. Chem. Soc. Dalton Trans.* 1993:2435–38
10. Wiley JB, Kaner RB. 1992. Rapid solid-state precursor synthesis of materials. *Science* 255:1093–97
11. Miki M, Yamasaki T, Ogino Y. 1992. Preparation of nanocrystalline NbN and (Nb,Al)N powders by mechanical alloying under nitrogen atmosphere. *Mater. Trans. Jpn. Inst. Metals* 33:839–44
12. Houmes JD, zur Loye HC. 1997. Microwave synthesis of ternary nitride materials. *J. Solid State Chem.* 130:266–71
13. Elder SH, Doerrer LH, DiSalvo FJ, Parise JB, Guyomard D, Tarascon JM. 1992. Lithium molybdenum nitride ($LiMoN_2$): the first metallic layered nitride. *Chem. Mater.* 4:928–37
14. Schnick W, Huppertz H. 1997. Nitridosilicates—a significant extension of silicate chemistry. *Chem. Eur. J.* 3:679–83
15. Langmi HW, McGrady GS. 2008. Ternary nitrides for hydrogen storage: Li–B–N, Li–Al–N and Li–Ga–N systems. *J. Alloys Compd.* 466:287–92
16. Javaid K, Yu J, Wu W, Wang J, Zhang H, et al. 2018. Thin film solar cell based on $ZnSnN_2$/SnO heterojunction. *Phys. Status Solidi* 12:1700332
17. Tellekamp MB, Melamed CL, Norman AG, Tamboli A. 2020. Heteroepitaxial integration of $ZnGeN_2$ on GaN buffers using molecular beam epitaxy. *Cryst. Growth Des.* 20:1868–75
18. Hinuma Y, Hatakeyama T, Kumagai Y, Burton LA, Sato H, et al. 2016. Discovery of earth-abundant nitride semiconductors by computational screening and high-pressure synthesis. *Nat. Commun.* 7:11962
19. Allen LC. 1989. Electronegativity is the average one-electron energy of the valence-shell electrons in ground-state free atoms. *J. Am. Chem. Soc.* 111:9003–14
20. Parr RG, Pearson RG. 1983. Absolute hardness: companion parameter to absolute electronegativity. *J. Am. Chem. Soc.* 105:7512–16
21. King R. 1995. The chemical bonding topology of ternary and quaternary transition metal nitrides containing low-coordinate metal atoms. *Can. J. Chem.* 73:963–71
22. Niewa R, DiSalvo FJ. 1998. Recent developments in nitride chemistry. *Chem. Mater.* 10:2733–52
23. Häglund J, Fernández Guillermet A, Grimvall G, Körling M. 1993. Theory of bonding in transition-metal carbides and nitrides. *Phys. Rev. B* 48:685–91
24. Marchand R, Laurent Y, Guyader J, L'Haridon P, Verdier P. 1991. Nitrides and oxynitrides: preparation, crystal chemistry and properties. *J. Eur. Ceram. Soc.* 8:197–213
25. Kniep R. 1997. Ternary and quaternary metal nitrides: a new challenge for solid state chemistry. *Pure Appl. Chem.* 69:185–92
26. Gregory DH. 1999. Structural families in nitride chemistry. *J. Chem. Soc. Dalton Trans.* 1999:259–70
27. Sun W, Holder A, Orvañanos B, Arca E, Zakutayev A, et al. 2017. Thermodynamic routes to novel metastable nitrogen-rich nitrides. *Chem. Mater.* 29:6936–46
28. Arca E, Lany S, Perkins JD, Bartel C, Mangum J, et al. 2018. Redox-mediated stabilization in zinc molybdenum nitrides. *J. Am. Chem. Soc.* 140:4293–301
29. Pamplin R. 1964. A systematic method of deriving new semiconducting compounds by structural analogy. *J. Phys. Chem. Solids* 25:675–84
30. Xia Z, Poeppelmeier KR. 2017. Chemistry-inspired adaptable framework structures. *Acc. Chem. Res.* 50:1222–30
31. Martinez AD, Fioretti AN, Toberer ES, Tamboli AC. 2017. Synthesis, structure, and optoelectronic properties of II–IV–V_2 materials. *J. Mater. Chem. A* 5:11418–35
32. Heinselman KN, Lany S, Perkins JD, Talley KR, Zakutayev A. 2019. Thin film synthesis of semiconductors in the Mg–Sb–N materials system. *Chem. Mater.* 31:8717–24
33. Sarmiento-Pérez R, Cerqueira TFT, Körbel S, Botti S, Marques MAL. 2015. Prediction of stable nitride perovskites. *Chem. Mater.* 27:5957–63
34. Talley KR, Perkins CL, Diercks DR, Brennecka GL, Zakutayev A. 2020. Synthesis of ferroelectric $LaWN_3$—the first nitride perovskite. arXiv:2001.00633 [cond-mat]

35. Szymanski NJ, Adhikari V, Willard MA, Sarin P, Gall D, Khare SV. 2019. Prediction of improved magnetization and stability in $Fe_{16}N_2$ through alloying. *J. Appl. Phys.* 126:093903
36. George NC, Denault KA, Seshadri R. 2013. Phosphors for solid-state white lighting. *Annu. Rev. Mater. Res.* 43:481–501
37. Mitchell B, Dierolf V, Gregorkiewicz T, Fujiwara Y. 2018. Perspective: toward efficient GaN-based red light emitting diodes using europium doping. *J. Appl. Phys.* 123:160901
38. Affleck I. 1981. Quantum-statistical metastability. *Phys. Rev. Lett.* 46:388–91
39. Anelli A, Engel EA, Pickard CJ, Ceriotti M. 2018. Generalized convex hull construction for materials discovery. *Phys. Rev. Mater.* 2:103804
40. Stevanović V. 2016. Sampling polymorphs of ionic solids using random superlattices. *Phys. Rev. Lett.* 116:075503
41. Sun W, Dacek ST, Ong SP, Hautier G, Jain A, et al. 2016. The thermodynamic scale of inorganic crystalline metastability. *Sci. Adv.* 2:e1600225
42. Bartel CJ, Millican SL, Deml AM, Rumptz JR, Tumas W, et al. 2018. Physical descriptor for the Gibbs energy of inorganic crystalline solids and temperature-dependent materials chemistry. *Nat. Commun.* 9:4168
43. Jain A, Ong SP, Hautier G, Chen W, Richards WD, et al. 2013. The Materials Project: a materials genome approach to accelerating materials innovation. *APL Mater.* 1:011002
44. Kroll P. 2003. Pathways to metastable nitride structures. *J. Solid State Chem.* 176:530–37
45. Aykol M, Dwaraknath SS, Sun W, Persson KA. 2018. Thermodynamic limit for synthesis of metastable inorganic materials. *Sci. Adv.* 4:eaaq0148
46. Greenaway AL, Loutris AL, Heinselman KN, Melamed CL, Schnepf RR, et al. 2020. Combinatorial synthesis of magnesium tin nitride semiconductors. *J. Am. Chem. Soc.* 142:8421–30
47. Singh AK, Zhou L, Shinde A, Suram SK, Montoya JH, et al. 2017. Electrochemical stability of metastable materials. *Chem. Mater.* 29:10159–67
48. Woods-Robinson R, Broberg D, Faghaninia A, Jain A, Dwaraknath SS, Persson KA. 2018. Assessing high-throughput descriptors for prediction of transparent conductors. *Chem. Mater.* 30:8375–89
49. Caskey C, Richards R, Ginley D, Zakutayev A. 2014. Thin film synthesis and properties of copper nitride, a metastable semiconductor. *Mater. Horiz.* 1:424–30
50. Siol S. 2019. Accessing metastability in heterostructural semiconductor alloys. *Phys. Status Solidi A* 216:1800858
51. von Alpen U, Rabenau A, Talat GH. 1977. Ionic conductivity in Li_3N single crystals. *Appl. Phys. Lett.* 30:621–23
52. Gregory DH. 2008. Lithium nitrides as sustainable energy materials. *Chem. Rec.* 8:229–39
53. Liu Y, Matsumura T, Imanishi N, Ichikawa T, Hirano A, Takeda Y. 2004. Lithium transition metal nitrides with the modified morphology characteristics as advanced anode materials for lithium ion batteries. *Electrochem. Commun.* 6:632–36
54. Cabana J, Stoeva Z, Titman JJ, Gregory DH, Palacín MR. 2008. Towards new negative electrode materials for Li-ion batteries: electrochemical properties of LiNiN. *Chem. Mater.* 20:1676–78
55. Zhu Y, He X, Mo Y. 2017. Strategies based on nitride materials chemistry to stabilize Li metal anode. *Adv. Sci.* 4:1600517
56. Verrelli R, Arroyo-de Dompablo ME, Tchitchekova D, Black AP, Frontera C, et al. 2017. On the viability of Mg extraction in $MgMoN_2$: a combined experimental and theoretical approach. *Phys. Chem. Chem. Phys.* 19:26435–41
57. Verrelli R, Black AP, Frontera C, Oró-Solé J, Arroyo-de Dompablo ME, et al. 2019. On the study of Ca and Mg deintercalation from ternary tantalum nitrides. *ACS Omega* 4:8943–52
58. Balogun MS, Qiu W, Wang W, Fang P, Lu X, Tong Y. 2015. Recent advances in metal nitrides as high-performance electrode materials for energy storage devices. *J. Mater. Chem. A* 3:1364–87
59. Yamane H, Okabe TH, Ishiyama O, Waseda Y, Shimada M. 2001. Ternary nitrides prepared in the Li_3N–Mg_3N_2 system at 900–1000 K. *J. Alloys Compd.* 319:124–30
60. Ischenko V, Kienle L, Jansen M. 2002. Formation and structure of $LiSi_2N_3$-AlN solid solutions. *J. Mater. Sci.* 37:5305–17

61. Hanghofer I, Brinek M, Eisbacher SL, Bitschnau B, Volck M, et al. 2019. Substitutional disorder: structure and ion dynamics of the argyrodites Li_6PS_5Cl, Li_6PS_5 Br and Li_6PS_5I. *Phys. Chem. Chem. Phys.* 21:8489–507
62. Saha S, Rousse G, Fauth F, Pomjakushin V, Tarascon JM. 2019. Influence of temperature-driven polymorphism and disorder on ionic conductivity in $Li_6Zn(P_2O_7)_2$. *Inorg. Chem.* 58:1774–81
63. Anasori B, Lukatskaya MR, Gogotsi Y. 2017. 2D metal carbides and nitrides (MXenes) for energy storage. *Nat. Rev. Mater.* 2:16098
64. Van de Walle C, Neugebauer J, Stampfl C, McCluskey M, Johnson N. 1999. Defects and defect reactions in semiconductor nitrides. *Acta Phys. Polon. A* 96:613–27
65. Melamed CL, Pan J, Mis A, Heinselman K, Schnepf RR, et al. 2020. Combinatorial investigation of structural and optical properties of cation-disordered $ZnGeN_2$. *J. Mater. Chem. C* 8:8736–46
66. Pan J, Cordell J, Tucker GJ, Tamboli AC, Zakutayev A, Lany S. 2019. Interplay between composition, electronic structure, disorder, and doping due to dual sublattice mixing in nonequilibrium synthesis of $ZnSnN_2$:O. *Adv. Mater.* 31:1807406
67. He X, Xiao Z, Katase T, Ide K, Hosono H, Kamiya T. 2019. Intrinsic and extrinsic defects in layered nitride semiconductor $SrTiN_2$. *J. Phys. Chem. C* 123:19307–14
68. Toyoura K, Oba F, Ninomiya T, Kuwabara A, Tanaka I. 2007. First-principles study of defect equilibria in lithium zinc nitride. *J. Phys. Condens. Matter* 19:046201
69. Yan Y, Wei SH. 2008. Doping asymmetry in wide-bandgap semiconductors: origins and solutions. *Phys. Status Solidi B* 245:641–52
70. Adamski NL, Zhu Z, Wickramaratne D, Van de Walle CG. 2019. Optimizing *n*-type doping of $ZnGeN_2$ and $ZnSiN_2$. *Phys. Rev. B* 100:155206
71. Adamski NL, Zhu Z, Wickramaratne D, Van de Walle CG. 2019. Strategies for p-type doping of $ZnGeN_2$. *Appl. Phys. Lett.* 114:032101
72. Fioretti AN, Zakutayev A, Moutinho H, Melamed C, Perkins JD, et al. 2015. Combinatorial insights into doping control and transport properties of zinc tin nitride. *J. Mater. Chem. C* 3:11017–28
73. Tsunoda N, Kumagai Y, Takahashi A, Oba F. 2018. Electrically benign defect behavior in zinc tin nitride revealed from first principles. *Phys. Rev. Appl.* 10:011001
74. Nakatsuka S, Nose Y. 2017. Order–disorder phenomena and their effects on bandgap in $ZnSnP_2$. *J. Phys. Chem. C* 121:1040–46
75. Schnepf RR, Levy-Wendt BL, Tellekamp MB, Ortiz BR, Melamed CL, et al. 2020. Using resonant energy X-ray diffraction to extract chemical order parameters in ternary semiconductors. *J. Mater. Chem. C* 8:4350–56
76. Bauers SR, Holder A, Sun W, Melamed CL, Woods-Robinson R, et al. 2019. Ternary nitride semiconductors in the rocksalt crystal structure. *PNAS* 116:14829–34
77. Haseman MS, Karim MR, Ramdin D, Noesges BA, Feinberg E, et al. 2020. Deep level defects and cation sublattice disorder in $ZnGeN_2$. *J. Appl. Phys.* 127:135703
78. Lany S, Fioretti AN, Zawadzki PP, Schelhas LT, Toberer ES, et al. 2017. Monte Carlo simulations of disorder in $ZnSnN_2$ and the effects on the electronic structure. *Phys. Rev. Mater.* 1:035401
79. Schnepf RR, Cordell JJ, Tellekamp MB, Melamed CL, Greenaway AL, et al. 2020. Utilizing site disorder in the development of new energy-relevant semiconductors. *ACS Energy Lett.* 5:2027–41
80. Hyot B, Rollès M, Miska P. 2019. Design of efficient type-II $ZnGeN_2/In_{0.16}Ga_{0.84}N$ quantum well-based red LEDs. *Phys. Status Solidi Rapid Res. Lett.* 13:1900170
81. Han L, Kash K, Zhao H. 2016. Designs of blue and green light-emitting diodes based on type-II InGaN-$ZnGeN_2$ quantum wells. *J. Appl. Phys.* 120:103102
82. Das B, Aguilera I, Rau U, Kirchartz T. 2020. What is a deep defect? Combining Shockley-Read-Hall statistics with multiphonon recombination theory. *Phys. Rev. Mater.* 4:024602
83. Luque A, Martí A, Stanley C. 2012. Understanding intermediate-band solar cells. *Nat. Photonics* 6:146–52
84. Luque A, Martí A, Antolín E, Tablero C. 2006. Intermediate bands versus levels in non-radiative recombination. *Physica B* 382:320–27
85. Gunning B, Lowder J, Moseley M, Doolittle WA. 2012. Negligible carrier freeze-out facilitated by impurity band conduction in highly p-type GaN. *Appl. Phys. Lett.* 101:082106

86. Javaid K, Wu W, Wang J, Fang J, Zhang H, et al. 2018. Band offset engineering in $ZnSnN_2$-based heterojunction for low-cost solar cells. *ACS Photonics* 5:2094–99
87. Karim MR, Jayatunga BHD, Zhu M, Lalk RA, Licata O, et al. 2020. Effects of cation stoichiometry on surface morphology and crystallinity of $ZnGeN_2$ films grown on GaN by metalorganic chemical vapor deposition. *AIP Adv.* 10:065302
88. Tsuji M, Hanzawa K, Kinjo H, Hiramatsu H, Hosono H. 2019. Heteroepitaxial thin-film growth of a ternary nitride semiconductor $CaZn_2N_2$. *ACS Appl. Electron. Mater.* 1:1433–38
89. Melamed CL, Tellekamp MB, Mangum JS, Perkins JD, Dippo P, et al. 2019. Blue-green emission from epitaxial yet cation-disordered $ZnGeN_{2-x}O_x$. *Phys. Rev. Mater.* 3:051602
90. Adamski NL, Zhu Z, Wickramaratne D. 2017. Hybrid functional study of native point defects and impurities in $ZnGeN_2$. *J. Appl. Phys.* 122:195701
91. Fioretti AN, Pan J, Ortiz BR, Melamed C, Dippo PC, et al. 2018. Exciton photoluminescence and benign defect complex formation in zinc tin nitride. *Mater. Horiz.* 5:823–30
92. Khan IS, Heinselman KN, Zakutayev A. 2020. Review of $ZnSnN_2$ semiconductor material. *J. Phys. Energy* 2:032007
93. Pan J, Cordell JJ, Tucker GJ, Zakutayev A, Tamboli AC, Lany S. 2020. Perfect short-range ordered alloy with line-compound-like properties in the $ZnSnN_2$:ZnO system. *npj Comput. Mater.* 6:63
94. Fioretti AN, Stokes A, Young MR, Gorman B, Toberer ES, et al. 2017. Effects of hydrogen on acceptor activation in ternary nitride semiconductors. *Adv. Electron. Mater.* 3:1600544
95. Lei T, Ludwig KF, Moustakas TD. 1993. Heteroepitaxy, polymorphism, and faulting in GaN thin films on silicon and sapphire substrates. *J. Appl. Phys.* 74:4430–37
96. Quayle PC, Blanton EW, Punya A, Junno GT, He K, et al. 2015. Charge-neutral disorder and polytypes in heterovalent wurtzite-based ternary semiconductors: the importance of the octet rule. *Phys. Rev. B* 91:205207
97. Kawamura F, Imura M, Murata H, Yamada N, Taniguchi T. 2020. Synthesis of a novel rocksalt-type ternary nitride semiconductor of $MgSnN_2$ using the metathesis reaction under high pressure. *Eur. J. Inorg. Chem.* 2020:446–51
98. Tareen AK, Priyanga GS, Behara S, Thomas T, Yang M. 2019. Mixed ternary transition metal nitrides: a comprehensive review of synthesis, electronic structure, and properties of engineering relevance. *Prog. Solid State Chem.* 53:1–26
99. Bale C, Chartrand P, Degterov S, Eriksson G, Hack K, et al. 2002. FactSage thermochemical software and databases. *Calphad* 26:189–228
100. Allison T. 1996. *NIST-JANAF thermochemical tables*. Data Tables, Natl. Inst. Stand. Technol. (NIST) Stand. Ref. Database 13, NIST, Washington, DC. **https://doi.org/10.18434/t42s31**
101. Mérel P, Tabbal M, Chaker M, Moisan M, Ricard A. 1998. Influence of the field frequency on the nitrogen atom yield in the remote plasma of an N_2 high frequency discharge. *Plasma Sources Sci. Technol.* 7:550–56
102. Iliopoulos E, Adikimenakis A, Dimakis E, Tsagaraki K, Konstantinidis G, Georgakilas A. 2005. Active nitrogen species dependence on radiofrequency plasma source operating parameters and their role in GaN growth. *J. Cryst. Growth* 278:426–30
103. Clinton EA, Vadiee E, Tellekamp MB, Doolittle WA. 2019. Observation and mitigation of RF-plasma-induced damage to III-nitrides grown by molecular beam epitaxy. *J. Appl. Phys.* 126:015705
104. Ong SP, Richards WD, Jain A, Hautier G, Kocher M, et al. 2013. Python Materials Genomics (pymatgen): a robust, open-source Python library for materials analysis. *Comput. Mater. Sci.* 68:314–19
105. Vajenine GV. 2007. Plasma-assisted synthesis and properties of Na_3N. *Inorg. Chem.* 46:5146–48
106. Caskey CM, Seabold JA, Stevanović V, Ma M, Smith WA, et al. 2015. Semiconducting properties of spinel tin nitride and other IV_3N_4 polymorphs. *J. Mater. Chem. C* 3:1389–96
107. Niewa R, Jacobs H, Mayer HM. 1995. Re-evaluation of the crystal structure of lithium zirconium nitride, Li_2ZrN_2, by neutron powder diffraction. *Z. Kristallogr.* 210:474–83
108. Hunting JL, Szymanski MM, Johnson PE, Brenhin Kellar C, DiSalvo FJ. 2007. The synthesis and structural characterization of the new ternary nitrides: Ca_4TiN_4 and Ca_5NbN_5. *J. Solid State Chem.* 180:31–40

109. Cabana J, Dupré N, Rousse G, Grey C, Palacín MR. 2005. Ex situ NMR and neutron diffraction study of structure and lithium motion in Li_7MnN_4. *Solid State Ion.* 176:2205–18
110. Niewa R, Zherebtsov DA, Schnelle W, Wagner FR. 2004. Metal-metal bonding in $ScTaN_2$. A new compound in the system ScN-TaN. *Inorg. Chem.* 43:6188–94
111. Bruls RJ, Hintzen HT, Metselaar R. 1999. Preparation and characterisation of $MgSiN_2$ powders. *J. Mater. Sci.* 34:4519–31
112. Blair RG, Anderson A, Kaner RB. 2005. A solid-state metathesis route to $MgSiN_2$. *Chem. Mater.* 17:2155–61
113. Maunaye M, Lang J. 1970. Preparation et propriétés de $ZnGeN_2$. *Mater. Res. Bull.* 5:793–96
114. Elder SH, DiSalvo FJ, Topor L, Navrotsky A. 1993. Thermodynamics of ternary nitride formation by ammonolysis: application to lithium molybdenum nitride ($LiMoN_2$), sodium tungsten nitride (Na_3WN_3), and sodium tungsten oxide nitride (Na_3WO_3N). *Chem. Mater.* 5:1545–53
115. Otsuka Y, Pitan C, Dornsieffer J, Takada T, Konoike T, Waser R. 2016. Synthesis of nitrogen and lanthanum codoped barium titanate with a novel thermal ammonolysis reactor. *J. Eur. Ceram. Soc.* 26:2719–25
116. Tessier F, Marchand R. 1997. An original way to prepare nitride-type compounds from sulfide precursors. *J. Alloys Compd.* 262/263:410–15
117. Lange H, Wötting G, Winter G. 1991. Silicon nitride—from powder synthesis to ceramic materials. *Angew. Chem. Int. Ed.* 30:1579–97
118. Rauch P, DiSalvo F, Brese N, Partin D, O'Keeffe M. 1994. Synthesis and neutron diffraction study of Na_3WN_3 and Na_3MoN_3. *J. Solid State Chem.* 110:162–66
119. Gillan EG, Kaner RB. 1994. Rapid solid-state synthesis of refractory nitrides. *Inorg. Chem.* 33:5693–700
120. Gillan EG, Kaner RB. 1996. Synthesis of refractory ceramics via rapid metathesis reactions between solid-state precursors. *Chem. Mater.* 8:333–43
121. Zakutayev A, Allen AJ, Zhang X, Vidal J, Cui Z, et al. 2014. Experimental synthesis and properties of metastable $CuNbN_2$ and theoretical extension to other ternary copper nitrides. *Chem. Mater.* 26:4970–77
122. Karpiński J, Jun J, Porowski S. 1984. Equilibrium pressure of N_2 over GaN and high pressure solution growth of GaN. *J. Cryst. Growth* 66:1–10
123. Aoki M, Yamane H, Shimada M, Sarayama S, DiSalvo FJ. 2001. Growth of 5 mm GaN single crystals at 750°C from an Na–Ga melt. *Cryst. Growth Des.* 1:119–22
124. Addison CC, Pulham RJ, Trevillion EA. 1975. Reaction between barium and nitrogen in liquid sodium: solubility studies. *J. Chem. Soc. Dalton Trans.* 1975:2082–85
125. Yamane H, DiSalvo FJ. 2018. Sodium flux synthesis of nitrides. *Prog. Solid State Chem.* 51:27–40
126. Yamane H, DiSalvo FJ. 1995. Synthesis and crystal structure of Sr_2ZnN_2 and Ba_2ZnN_2. *J. Solid State Chem.* 119:375–79
127. Yamane H, DiSalvo FJ. 1996. A barium germanium nitride, $Ba_3Ge_2N_2$, containing $\frac{1}{x}|Ge^{2-}$ and $\frac{1}{x}GeN_2^{4-}$ anions. *J. Alloys Compd.* 241:69–74
128. Dickman MJ, Latturner SE. 2016. Metal nitrides grown from Ca/Li flux: $Ca_6Te_3N_2$ and new nitridoferrate(I) $Ca_6(Li_xFe_{1-x})Te_2N_3$. *J. Am. Chem. Soc.* 138:10636–44
129. Wang B, Callahan MJ. 2006. Ammonothermal synthesis of III-nitride crystals. *Cryst. Growth Des.* 6:1227–46
130. Richter TM, Niewa R. 2014. Chemistry of ammonothermal synthesis. *Inorganics* 2:29–78
131. Häusler J, Schnick W. 2018. Ammonothermal synthesis of nitrides: recent developments and future perspectives. *Chem. Eur. J.* 24:11864–79
132. Häusler J, Niklaus R, Minár J, Schnick W. 2018. Ammonothermal synthesis and optical properties of ternary nitride semiconductors Mg-IV-N_2, Mn-IV-N_2 and Li-IV_2-N_2 (IV=Si,Ge). *Chem. Eur. J.* 24:1686–93
133. Borg RJ, Dienes GJ. 1988. *An Introduction to Solid State Diffusion*. San Diego, CA: Academic
134. Endo T, Sato Y, Takizawa H, Shimada M. 1992. High-pressure synthesis of new compounds, $ZnSiN_2$ and $ZnGeN_2$ with distorted wurtzite structure. *J. Mater. Sci. Lett.* 11:424–26
135. Kawamura F, Yamada N, Imai M, Taniguchi T. 2016. Synthesis of $ZnSnN_2$ crystals via a high-pressure metathesis reaction. *Cryst. Res. Technol.* 51:220–24

136. Du K, Bekele C, Hayman C, Angus J, Pirouz P, Kash K. 2008. Synthesis and characterization of $ZnGeN_2$ grown from elemental Zn and Ge sources. *J. Cryst. Growth* 310:1057–61
137. Quayle PC, He K, Shan J, Kash K. 2013. Synthesis, lattice structure, and band gap of $ZnSnN_2$. *MRS Commun.* 3:135–38
138. Quayle PC, Junno GT, He K, Blanton EW, Shan J, Kash K. 2017. Vapor-liquid-solid synthesis of $ZnSnN_2$. *Phys. Status Solidi B* 254:1600718
139. Grekov FF, Chernovets BV. 2004. Methods for $MgSiN_2$ synthesis. *Russ. J. Appl. Chem.* 77:1223–26
140. Ptak AJ, Millecchia MR, Myers TH, Ziemer KS, Stinespring CD. 1999. The relation of active nitrogen species to high-temperature limitations for $(000\bar{1})$ GaN growth by radio-frequency-plasma-assisted molecular beam epitaxy. *Appl. Phys. Lett.* 74:3836–38
141. Blant AV, Hughes OH, Cheng TS, Novikov SV, Foxon CT. 2000. Nitrogen species from radio frequency plasma sources used for molecular beam epitaxy growth of GaN. *Plasma Sources Sci. Technol.* 9:12–17
142. Thornton JA. 1974. Influence of apparatus geometry and deposition conditions on the structure and topography of thick sputtered coatings. *J. Vac. Sci. Technol.* 11:666–70
143. Arakawa Y, Ueno K, Kobayashi A, Ohta J, Fujioka H. 2016. High hole mobility p-type GaN with low residual hydrogen concentration prepared by pulsed sputtering. *APL Mater.* 4:086103
144. Umeda K, Takeuchi M, Yamada H, Kubo R, Yoshino Y. 2006. Improvement of thickness uniformity and crystallinity of AlN films prepared by off-axis sputtering. *Vacuum* 80:658–61
145. Howson RP. 1994. The reactive sputtering of oxides and nitrides. *Pure Appl. Chem.* 66:1311–18
146. McGinn PJ. 2019. Thin-film processing routes for combinatorial materials investigations—a review. *ACS Comb. Sci.* 21:501–15
147. Lide DR, ed. 1993. *CRC Handbook of Chemistry & Physics*. Boca Raton, FL: CRC. 74th ed.
148. Feldberg N, Aldous JD, Linhart WM, Phillips LJ, Durose K, et al. 2013. Growth, disorder, and physical properties of $ZnSnN_2$. *Appl. Phys. Lett.* 103:042109
149. Mizuta M, Fujieda S, Matsumoto Y, Kawamura T. 1986. Low temperature growth of GaN and AlN on GaAs utilizing metalorganics and hydrazine. *Jpn. J. Appl. Phys.* 25:L945–48
150. Koukitu A, Kumagai Y, Kubota N, Seki H. 1999. Thermodynamic analysis on the MOVPE growth of nitride semiconductors using hydrazine. *Phys. Status Solidi B* 216:707–12
151. Zhu LD, Maruska PH, Norris PE, Yip PW, Bouthillette LP. 1999. Epitaxial growth and structural characterization of single crystalline $ZnGeN_2$. *MRS Online Proc. Libr.* 537:38
152. Misaki T, Wakahara A, Okada H, Yoshida A. 2004. Epitaxial growth and characterization of $ZnGeN_2$ by metalorganic vapor phase epitaxy. *J. Cryst. Growth* 260:125–29
153. Larson WL, Maruska HP, Stevenson DA. 1974. Synthesis and properties of $ZnGeN_2$. *J. Electrochem. Soc.* 121:1673–74
154. Lany S. 2013. Band-structure calculations for the 3d transition metal oxides in GW. *Phys. Rev. B* 87:085112
155. Sands T, Palmström CJ, Harbison JP, Keramidas VG, Tabatabaie N, et al. 1990. Stable and epitaxial metal/III-V semiconductor heterostructures. *Mater. Sci. Rep.* 5:99–170
156. Baliga BJ. 1982. Semiconductors for high-voltage, vertical channel field-effect transistors. *J. Appl. Phys.* 53:1759–64
157. Coltrin ME, Kaplar RJ. 2017. Transport and breakdown analysis for improved figure-of-merit for AlGaN power devices. *J. Appl. Phys.* 121:055706
158. Adamski NL, Wickramaratne D, Van de Walle CG. 2020. Band alignments and polarization properties of the Zn-IV-nitrides. *J. Mater. Chem. C* 8:7890–98
159. Akiyama M, Kamohara T, Kano K, Teshigahara A, Takeuchi Y, Kawahara N. 2009. Enhancement of piezoelectric response in scandium aluminum nitride alloy thin films prepared by dual reactive cosputtering. *Adv. Mater. Commun.* 21:593–96
160. Fichtner S, Wolff N, Lofink F, Kienle L, Wagner B. 2019. AlScN: a III-V semiconductor based ferroelectric. *Appl. Phys.* 125:114103
161. Jena D, Page R, Casamento J, Dang P, Singhal J, et al. 2019. The new nitrides: layered, ferroelectric, magnetic, metallic and superconducting nitrides to boost the GaN photonics and electronics eco-system. *Jpn. J. Appl. Phys.* 58:SC0801

162. Unverfehrt L, Glaser J, Stroebele M, Tragl S, Gibson K, Meyer HJ. 2009. The versatility of solid-state metathesis reactions: from rare earth fluorides to carboiimides. *Z. Anorg. Allg. Chem.* 635:479–83
163. Hosono A, Stoffel RP, Masubuchi Y, Dronskowski R, Kikkawa S. 2019. Melting behavior of alkaline-earth metal carbodiimides and their thermochemistry from first principles. *Inorg. Chem.* 58:8938–42
164. Odahara J, Sun W, Miura A, Rosero-Navarro NC, Nagao M, et al. 2019. Self-combustion synthesis of novel metastable ternary molybdenum nitrides. *ACS Mater. Lett.* 1:64–70
165. Alvarez D, Spiegelman J, Andachi K, Holmes R, Raynor M, Shimizu H. 2017. Enabling low temperature metal nitride ALD using ultra-high purity hydrazine: ET/ID: enabling technologies and innovative devices. In *Proceedings of the 2017 28th Annual SEMI Advanced Semiconductor Manufacturing Conference (ASMC)*, pp. 426–30. Piscataway, NJ: IEEE
166. Houmes JD, zur Loye HC. 1996. Plasma nitridation of metal oxides. *Chem. Mater.* 8:2551–53
167. Saha B, Shakouri A, Sands TD. 2018. Rocksalt nitride metal/semiconductor superlattices: a new class of artificially structured materials. *Appl. Phys. Rev.* 5:021101